GEOLOGY OF THE INTERMOUNTAIN WEST
an open-access journal of the Utah Geological Association
ISSN 2380-7601
Volume 5 *2018*

NEW INSIGHTS ON THE IMPACT OF TIDAL CURRENTS ON A LOW-GRADIENT, SEMI-ENCLOSED, EPICONTINENTAL BASIN—THE CURTIS FORMATION, EAST-CENTRAL UTAH, USA

Valentin Zuchuat, Arve R.N. Sleveland, Douglas A. Sprinkel, Algirdas Rimkus, Alvar Braathen, and Ivar Midtkandal

GEOLOGY OF THE INTERMOUNTAIN WEST

an open-access journal of the Utah Geological Association

ISSN 2380-7601

Volume 5 ***2018***

Editors

Douglas A. Sprinkel
Utah Geological Survey
801.391.1977
GIW@utahgeology.org

Thomas C. Chidsey, Jr.
Utah Geological Survey
801.537.3364
tomchidsey@utah.gov

Bart J. Kowallis
Brigham Young University
801.422.2467
bkowallis@gmail.com

Steven Schamel
GeoX Consulting, Inc.
801.583-1146
geox-slc@comcast.net

Production

Cover Design and Desktop Publishing
Douglas A. Sprinkel

Cover

View from the Lower South Desert Overlook, Capitol Reef National Park, displaying the earthy facies of the Callovian Entrada Sandstone (reddish-colored sandstone), overlain by the Oxfordian, tidally influenced Curtis Formation (light-colored sandstone). The two units are separated by the J-3 unconformity, which coincides here with the Major Transgressive Surface (MTS) at the base of the informal middle Curtis. Note the evidences of tidal ravinement at the base of the middle Curtis. The middle Curtis consists mainly very fine to fine-grained sandstone, and corresponds to a sub- to intertidal channel-dune-flat complex depositional setting. The middle Curtis gradually grades into the thinner-bedded, very fine-grained, sub- to intertidal heterolithic flat deposits of the upper Curtis, which is conformably overlain by the Summerville Formation. Note the geologist in the lower right quadrant of the photograph for scale.

UGA Board

2018 President	Paul Inkenbrandt	paulinkenbrandt@utah.gov	801.537.3361
2018 President-Elect	Peter Nielsen	peternielsen@utah.gov	801.537.3359
2018 Program Chair	Emily McDermott	emcdermott@utah.gov	801.537.3389
2018 Treasurer	Zach Anderson	zanderson@utah.gov	801.538.4779
2018 Secretary	Christopher Kravits	ckravitsgeo@gmail.com	
2018 Past President	Bill Loughlin	bill@loughlinwater.com	435.649.4005

UGA Committees

Education/Scholarship	Loren Morton	lmorton@utah.gov	801.536.4262
Environmental Affairs	Craig Eaton	eaton@ihi-env.com	801.633.9396
Geologic Road Sign	Terry Massoth	twmassoth@hotmail.com	801.541.6258
Historian	Paul Anderson	paul@pbageo.com	801.364.6613
Membership	Rick Ford	rford@weber.edu	801.626.6942
Public Education	Paul Jewell	pwjewell@mines.utah.edu	801.581.6636
	Matt Affolter	gfl247@yahoo.com	
Publications	Roger Bon	rogerbon@xmission.com	801.942.0533
Publicity	Paul Inkenbrandt	paulinkenbrandt@utah.gov	801.537.3361
Social/Recreation	Roger Bon	rogerbon@xmission.com	801.942.0533

AAPG House of Delegates

2017–2020 Term	Tom Chidsey	tomchidsey@utah.gov	801.537.3364

State Mapping Advisory Committe

UGA Representative	Jason Blake	blake-j@comcast.net	435.658.3423

Earthquake Safety Committe

Chair	Grant Willis	gwillis@utah.gov	801.537.3355

UGA Website
www.utahgeology.org

Webmasters	Paul Inkenbrandt	paulinkenbrandt@utah.gov	801.537.3361
	Lance Weaver	lanceweaver@utah.gov	801.403.1636

UGA Newsletter

Newsletter Editor	Bill Lund	uga.newsletter@gmail.com	435.590.1338

Become a member of the UGA to help support the work of the Association and receive notices for monthly meetings, annual field conferences, and new publications. Annual membership is $20 and annual student membership is only $5. Visit the UGA website at www.utahgeology.org for information and membership application.

The UGA board is elected annually by a voting process through UGA members. However, the UGA is a volunteer-driven organization, and we welcome your voluntary service. If you would like to participate please contact the current president or committee member corresponding with the area in which you would like to volunteer.

Utah Geological Association formed in 1970 from a merger of the Utah Geological Society, founded in 1946, and the Intermountain Association of Geologists, founded in 1949. Affiliated with the American Association of Petroleum Geologists.

GEOLOGY OF THE INTERMOUNTAIN WEST
an open-access journal of the Utah Geological Association

Volume 5 ***2018***

New Insights on the Impact of Tidal Currents on a Low-gradient, Semi-enclosed, Epicontinental Basin—the Curtis Formation, East-central Utah, USA

Valentin Zuchuat[1], Arve R.N. Sleveland[1], Douglas A. Sprinkel[2], Algirdas Rimkus[1], Alvar Braathen[1], Ivar Midtkandal[1]

[1] University of Oslo, Department of Geosciences, Sem Sælands vei 1, 0371, Oslo, Norway; valentin.zuchuat@geo.uio.no
[2] Utah Geological Survey, PO Box 146100, Salt Lake City, Utah 84114; douglassprinkel@utah.gov

ABSTRACT

Based on a methodic sedimentological analysis, the Late Jurassic (Oxfordian) Curtis Formation unravels the intricate facies variability which occurs in a tide-dominated, fluvially starved, low-gradient, semi-enclosed epicontinental basin. This unit crops out in east-central Utah, between the eolian deposits of the underlying Middle Jurassic (Callovian) Entrada Sandstone, from which it is separated by the J-3 unconformity, and the conformable overlying supratidal Summerville Formation of Oxfordian age. A high-resolution sedimentary analysis of the succession led to the recognition of eight facies associations (FA) with six sub-facies associations. Based on the specific three-dimensional arrangement of these eight facies associations, it is proposed to separate the Curtis Formation into three sub-units: the lower, middle and upper Curtis. The J-3 unconformity defines the base of the lower Curtis, which consists of upper shoreface to beach deposits (FA 2), mud-dominated (FA 3a) and sand-dominated heterolithic subtidal flat (FA 3b), sand-rich sub- to supratidal flat (FA 4a) and correlative tidal channel infill (FA 4c). It is capped by the middle Curtis, which coincides with the sub- to intertidal channel-dune-flat complex of FA 5, and its lower boundary corresponds to a transgressive surface of regional extent, identified as the Major Transgressive Surface (MTS). This surface suggests a potential correlation between the middle and the upper Curtis and the neighboring Todilto Member of the Wanakah Formation or Todilto Formation. The upper Curtis consists of the heterolithic upper sub- to intertidal flat (FA 6) and coastal dry eolian dunes belonging to the Moab Member of the Curtis Formation (FA 7), and it conformably overlies the middle Curtis.

The spatial distribution of these sub-units supports the distinction of three different sectors across the study area: sector 1 in the north, sector 2 in the south-southwest, and sector 3 in the east. In sector 1, the Curtis Formation is represented by its three sub-units, whereas sector 2 is dominated by the middle and upper Curtis, and sector 3 encompasses the extent of the Moab Member of the Curtis Formation.

This study also highlights the composite nature of the J-3 unconformity, which was impacted by various processes occurring before the Curtis Formation was deposited, as well as during the development of the lower and middle Curtis. Local collapse features within the lower and middle Curtis are linked to sand fluid overpressure within a remobilized sandy substratum, potentially triggered by seismic activity. Furthermore, the occurrence of a sub-regional angular relationship between the middle Curtis and substratum implies that the area of study was impacted by a regional deformational event during the Late Jurassic, before the deposition of the middle Curtis.

Citation for this article.
Zuchuat, V., Sleveland, A.R.N., Sprinkel, D.A., Rimkus, A., Braathen, A., and Midtkandal, I., 2018, New insights on the impact of tidal currents on a low-gradient, semi-enclosed, epicontinental basin—the Curtis Formation, east-central Utah, USA: Geology of the Intermountain West, v. 5, p. 131–165.

INTRODUCTION

The complex aspect of tide-dominated environments was reported as early as first century AD, when Pliny the Elder, in his *Historia Naturalis*, wondered whether such areas "invaded twice each day and night by the overflowing waves of the ocean…are to be looked upon as belonging to the land, or whether as forming portion of the sea?" (translation from Bostock and Riley, 1855). Since then, it has been shown that the essence of tidal deposits resides within their typical three-dimensional intricate assemblage of heterolithic facies, which distribution is dictated by a fine equilibrium of sediment input, basinal hydrodynamic forces, as well as avulsing and migrating channels (Davis and Dalrymple, 2012; references therein). This complexity is further enhanced by temporal and cyclical variations of tidal currents in a basin, which unevenly impact the erosion-transport-deposition mechanisms of the different grain classes within the system (Kvale, 2012; Wang, 2012; references therein). Adding to the intrinsically dynamic system, the effects of fluctuating rates in relative sea-level variation are amplified by a low-gradient shelf through shifting facies belts over great distances (Midtkandal and Nystuen, 2009). Poor time constraints, limited but changing accommodation, and pre-existing basin floor relief further complicate the accurate interpretation and correlation of such deposits. Despite highly complex depositional scenarios, these conditions may produce substantial volumes of reservoir-grade sandstone, and represent potentially viable aquifers, CO_2-injection targets, or petroleum reservoirs (Martinius and others, 2005; Halland and others, 2014).

Research focusing on siliciclastic tide-dominated environments recognizes four main categories: (1) the upward fining, transgressive estuarine, (2) the (semi-)protected lagoonal systems, (3) the prograding tide-dominated deltas, as well as (4) the open-coast tidal flats (e.g., Boyd and others, 1992; Dalrymple and others, 1992; Fan, 2012). Whereas modern analogs can help scientists identifying such depositional systems in the rock record, Tape and others (2003) highlighted the fact that some tidally influenced sedimentary units do not belong to any of the above-mentioned classes and cannot be illustrated by modern equivalent environments either, as they were deposited on broad and shallow epicontinental shelves. The outstanding outcrop quality and the significant internal variability of the Middle Jurassic Entrada Sandstone and Late Jurassic Curtis-Summerville Formations of east-central Utah allow a detailed investigation of gradual, subtle, and intricate interactions within such a low-gradient, continental to subtidal epeiric system, characterized by a starvation of major fluvial input (Kreisa and Moiola, 1986; Caputo and Pryor, 1991; Wilcox and Currie, 2008). The main objective of this study is to develop a detailed data-driven classification of heterolithic facies and facies associations present on a tidally influenced siliciclastic-dominated shelf of regional extent, represented by the Curtis Formation of Early Oxfordian age (about 161–159 Ma) (Kreisa and Moiola, 1986; Caputo and Pryor, 1991; Wilcox and Currie, 2008; Ogg and others, 2016). This work establishes the sedimentary basis for deconstructing the growth and infill dynamic of such a tide-dominated basin, which will be analyzed in a separate study. The overarching goal of this venture is to generate a multi-disciplinary predictive protocol to assess the combined seal-reservoir properties of such heterolithic deposits, notably for carbon capture and storage purposes.

GEOLOGICAL SETTING

Basinal Setting

Since the Mesozoic, Utah's geological history has been profoundly influenced by several tectonic events, markedly by the development of the North American Cordillera and its cascade of orogenies; key orogenies, partly overlapping in time and space (Bump and Davis, 2003; Hintze and Kowallis, 2009; Thorman, 2011; Anderson, 2015; Yonkee and Weil, 2015; and references therein), are (1) the Middle Jurassic-Early Cretaceous Nevadan orogeny, whose remains notably consist of small granitic batholiths at today's Utah-Nevada border, (2) the Middle Jurassic Elko orogeny, which differs from the other orogenies by alternating extensional and contractional tectonic events, (3) the Early Cretaceous to Paleogene Sevier orogeny, with its resultant thin-skinned contractional structures associated with a fore-

land basin development, and (4) the Late Cretaceous to Paleogene Laramide orogeny seen as basement-rooted monoclines, from which the San Rafael Swell and other large uplifts emerged. Additionally, rocks from east-central to southeastern Utah were also affected by movements of the Paradox Basin salt deposits (Trudgill, 2011), regional uplifts of the Colorado Plateau, and related extensional events (Levander and others, 2011; Murray and others, 2016). There were also intrusive and extrusive magmatic episodes during the Middle to Late Oligocene; the latter are expressed by the Henry, La Sal, and Abajo Mountains igneous complexes (Sullivan and others, 1991; Nelson, 1997). Burial history data compiled by Nuccio and Condon (1996) and Petrie and others (2017) suggest that the Curtis Formation was buried to depths of 2.45 km and 2.86 km near the San Rafael Swell.

Stratigraphy

The westward-thickening sedimentary succession of the San Rafael Group was deposited in neighboring areas of the Utah-Idaho trough, a north-northeast to south-southwest-trending distal retroarc foreland basin parallel to the Elko highlands (figure 1) (Anderson and Lucas, 1994; Brenner and Peterson, 1994; Peterson, 1994; Bjerrum and Dorsey, 1995; Thorman, 2011). This basin recorded multiple transgressive-regressive marine cycles (Anderson and Lucas, 1994). The marine and intertonguing eolian sediments of the coastal paleo-erg of the Middle Jurassic (Aalenian to Bajocian) Temple Cap Formation in southwestern and central Utah unconformably overlies the eolian Navajo Sandstone of Early Jurassic age on the J-1 unconformity (Pipiringos and O'Sullivan, 1978; Peterson and Pipiringos, 1979; Sprinkel and others, 2011). Paleowind indicators for the Navajo Sandstone suggest a north-northwest to south-southeast wind direction, whereas paleowind indicators for the Temple Cap Formation suggest a northeast to southwest wind direction (Parrish and Peterson, 1988; Peterson, 1988; Hartwick, 2010). To the east in south-central Utah, the former basal Harris Wash Member of the Page Sandstone unconformably overlies the Navajo Sandstone, above the J-2 unconformity of Pipiringos and O'Sullivan (1978) and Peterson and Pipiringos (1979). Isotopic ages obtained from ash beds in the Harris Wash Member indicated they were time equivalent to the Temple Cap Formation and hence pre-dated the basal Carmel Formation (Kowallis and others, 2001; Dickinson and others, 2010; Sprinkel and others, 2011). This stratigraphic relationship brought into question the validity of the J-2 unconformity and led to the recommendation to re-assign the beds representing the Harris Wash Member of the Page Sandstone to the Temple Cap Formation (Sprinkel and others, 2011; Doelling and others, 2013). The shallow marine Middle Jurassic Carmel Formation (Gilluly and Reeside, 1928) conformably overlies the Temple Cap Formation, reflecting marine incursions from the northern Sundance seaway from Bajocian to early Callovian time (Anderson and Lucas, 1994; Brenner and Peterson, 1994; Peterson, 1994; Hintze and Kowallis, 2009; Sprinkel and others, 2011). However, the Carmel Formation does unconformably overlie the Navajo Sandstone in places where the Temple Cap Formation is missing because of irregular deposition of the Temple Cap on a pre-existing paleotopography and its depositional pinch-out in eastern Utah (Sprinkel and others, 2011; Doelling and others, 2013).

Continental conditions returned with the deposition of the Middle Jurassic (Callovian) Entrada Sandstone (Peterson, 1994: Hintze and Kowallis, 2009), formally defined by Gilluly and Reeside (1928). This sedimentary formation is divided into two units: (1) the basal Slick Rock Member, which consists of alternating eolian dune and interdune intervals, and (2) the overlying informal, intermittently vegetated, earthy facies, which was deposited in a marginal marine setting (Witkind, 1988; Crabaugh and Kocurek, 1993; Carr-Crabaugh and Kocurek, 1998; Mountney, 2012; Doelling and others, 2015). The Entrada Sandstone and correlative formations (Twist Gulch and Preuss Formations) thicken westward towards the Utah-Idaho trough and northwards towards the Sundance Seaway (Imlay, 1980; Kocurek and Dott, 1983). Dickinson and Gehrels (2009, 2010) showed that the siliciclastic grains of the Entrada Sandstone were mostly recycled from river systems sourced from the Appalachian Mountains, on the eastern side of the continent.

The Entrada Sandstone recorded four erg con-

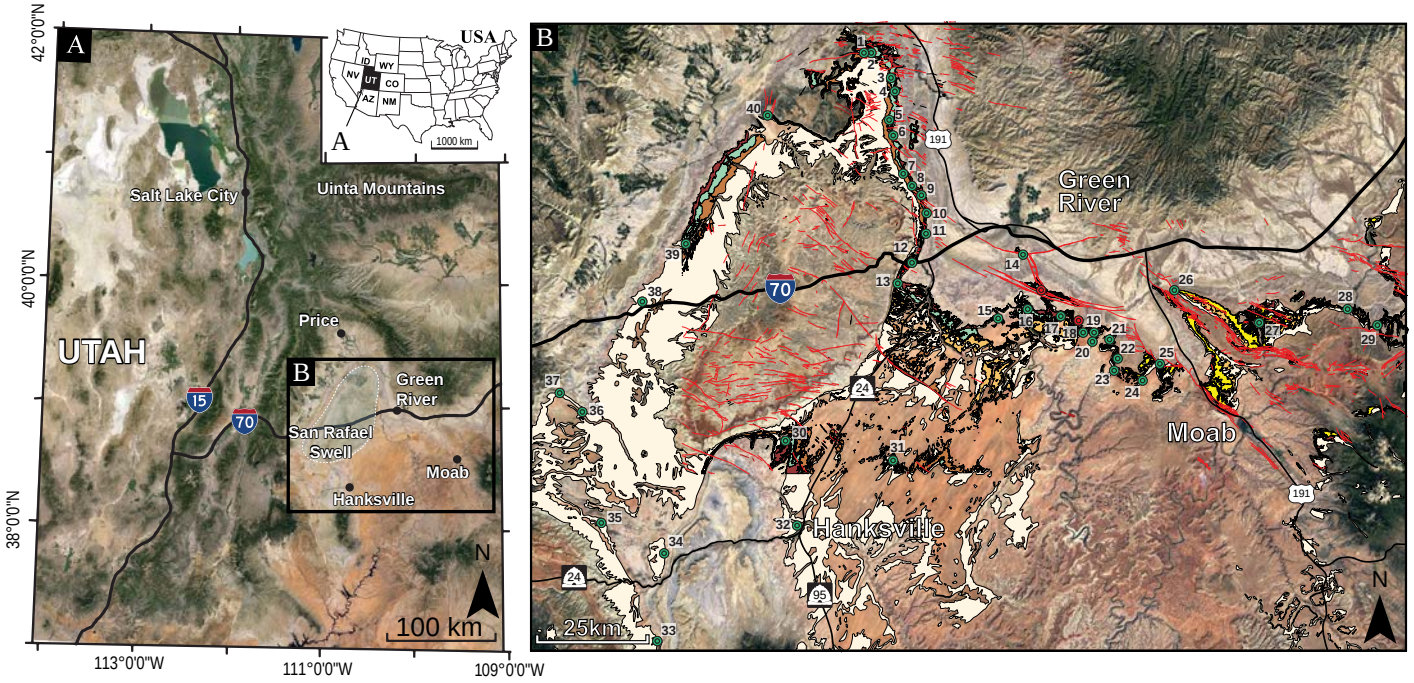

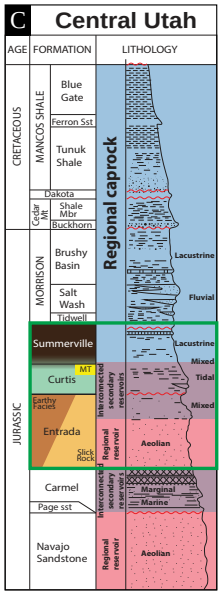

Log N°	Log name	Date	UTM - coordinates			Log N°	Log name	Date	UTM - coordinates		
			Grid	Easting	Northing				Grid	Easting	Northing
1	Sulphur Canyon	27.06.2015	12 S	538598	4354691	21	Ten Mile Rd	28.05.2016	12 S	594368	4291828
2	Stove Gulch East	23.06.2015	12 S	541150	4354677	22	Petrified Tree Gulch	29.05.2016	12 S	596564	4287509
3	Humbug Flats East	30.06.2015	12 S	545496	4349054	23	Dubinky Well Rd	27.05.2016	12 S	595351	4284912
4	Neversweat Wash	01.07.2015	12 S	546582	4345984	24	Safari Road	26.05.2016	12 S	601764	4282137
5	Middle Canyon	21.09.2015	12 S	545582	4340631	25	Bartlett Wash	16.06.2015	12 S	605257	4286436
6	Dry Mesa	02.07.2015	12 S	546370	4336290	26	Salt Valley	21.05.2016	12 S	608768	4302663
7	Curtis Point	03.05.2016	12 S	549241	4328385	27	Lost Spring Canyon	23.05.2016	12 S	624118	4294979
8	Wet Gulch	04.05.2016	12 S	550874	4325353	28	Dewey Bridge	10.05.2016	12 S	647467	4298329
9	Sven's Gulch	22.09.2015	12 S	552531	4323706	29	Big Pinto Mesa	22.05.2016	12 S	654182	4294917
10	Smith's Cabin	03.07.2015	12 S	553584	4319583	30	Goblin Valley	29.04.2017	12 S	522572	4269001
11	Rabbit Gulch	19.05.2016	12 S	553369	4314960	31	Little Flat Top	08.05.2016	12 S	544488	4266008
12	Interstate 70	06.05.2016	12 S	550457	4308362	32	Hanksville	05.05.2017	12 S	525317	4248736
13	Uneva Mine Canyon	12.05.2016	12 S	547594	4304403	33	Notom Ranch	09.05.2017	12 S	492291	4226559
14	Crystal Geyser	15.09.2015	12 S	575060	4310623	34	Cainville Airstrip	11.05.2017	12 S	495813	4244029
15	Lower San Rafael Rd	20.05.2016	12 S	570049	4295643	35	L. South Desert Ov.	12.05.2017	12 S	481839	4250657
16	Ruby Ranch Meandre	04.06.2016	12 S	576420	4298161	36	LCD the Two Towers	27.04.2017	12 S	477493	4275207
17	Ruby Ranch Road	03.06.2016	12 S	583113	4296930	37	LCD Road Cut	25.04.2017	12 S	472428	4279105
18	Duma Point	01.06.2016	12 S	588894	4293333	38	Salt Wash View Area	16.05.2017	12 S	490555	4298727
19	Horse Flies Gulch	31.05.2016	12 S	590606	4293184	39	Sid and Charley	15.05.2017	12 S	500015	4311719
20	Dune Mesa	30.05.2016	12 S	590620	4290953	40	Lower Cedar Mt Rd	14.05.2017	12 S	518557	4340815

Figure 1. (A) Maps of the study area. (B) Green dots represent visited localities where the Curtis Formation crops out, whereas red dots (not numbered) illustrate its absence. Each dot number on the map refers to a specific locality in the attached table (geological units after Hintze, 1980; Witkind, 1988; Doelling, 2001; and Doelling and others, 2015). (C) Schematic stratigraphic column of the area (modified from Ogata and others, 2014).

struction-destruction cycles (sensu Mountney, 2006), dictated by regional variations of the paleo-water table, themselves related to relative sea level fluctuations (Carr-Crabaugh and Kocurek, 1998; Mountney, 2012). The entire system is truncated along its top by the regional J-3 unconformity (Pipiringos and O'Sullivan, 1978; Hintze and Kowallis, 2009), with local relief of up to about 23 m. In areas of south-central Utah, the J-3 unconformity truncates subtle, large-amplitude folds developed in the Entrada Sandstone and underlying formations, exhibiting distinctive angular relationships along the unconformity (see figure 7 of Wheatley and

others, 2016). Depending on location, this boundary can be characterized as a conformable contact, a paraconformity, a disconformity, or an angular unconformity. It is important to note that the precise time encapsulated in the composite J-3 unconformity remains unknown. Since the definition of an unconformity implies a "lacuna of substantial duration" (sensu Holbrook and Bhattacharya, 2012), the nature of the J-3 unconformity remains a point of discussion. Peterson (1994) argued that a regional tectonic uplift in the west played the major role in the development of this unconformity, whereas Caputo and Pryor (1991) as well as Eschner and Kocurek (1988), respectively, advocated that (unidentified) marine or tidal currents during the earliest stage of the Curtis transgression reworked the substratum.

The overlying tidally influenced Curtis Formation of Early Oxfordian age (Kreisa and Moiola, 1986; Caputo and Pryor, 1991; Wilcox and Currie, 2008; Ogg and others, 2016) was first formally defined by Gilluly and Reeside (1928), and its type section of Curtis Point is located about 5.3 km south of Dry Mesa, along the northeastern margin of the San Rafael Swell (UTM coordinates: 12S 547430/4331169). The formation is characterized by its greenish-whitish color due to the presence of glauconite or chlorite (Gilluly and Reeside, 1928; Caputo and Pryor, 1991; Peterson, 1994). Its striking color contrast to the underlying earthy red Entrada Sandstone is readily identifiable in outcrops. The typical thickness ranges between 30 and 80 m around the San Rafael Swell (Caputo and Pryor, 1991). Nevertheless, as it was deposited in the foredeep basin of the Elko orogeny (Thorman, 2011; Anderson, 2015), the formation pinches out southwards towards Tergeson Flats, about 38 km southwest of Hanksville, as well as eastwards in the vicinity of Duma Point, about 28 km south-southeast of Green River (figure 1) (Gilluly and Reeside, 1928; Caputo and Pryor, 1991; Peterson, 1994). As a note, the coastal paleo-erg of the Moab Member of the Curtis Formation is the lateral equivalent to the marine beds of the Curtis towards the east of the study area (Wright and others, 1962; Caputo and Pryor, 1991; Peterson, 1994; Doelling, 2001).

The Summerville Formation conformably overlies the Curtis Formation in the San Rafael Swell and Henry Mountains basin and is characterized by dark-red and chocolate-brown hypersaline sabkha deposits, including evaporative ponds, which resulted in precipitation of gypsum and anhydrite (Gilluly and Reeside, 1928; Caputo and Pryor, 1991; Peterson, 1994; Lucas, 2014). Peterson (1994) described the marine Curtis Formation and the conformably overlying supra-tidal and sabkha deposits of the Summerville Formation as representing the fifth transgressive-regressive cycle within the Jurassic System of the Western Interior basin. This cycle potentially corresponds to Haq and others (1987) LZA-2.3 third-order transgressive-regressive interval, after calibrating their curve onto Wilcox and Currie (2008) age and Ogg and others (2016) time scale. The Curtis-Summerville interval correlates to the Redwater Shale Member of the Sundance Formation (Imlay 1947, 1980) in Wyoming, the Stump Formation around the Wyoming-Idaho border (Mansfield and Roundy, 1916; Pipiringos and Imlay, 1979; Imlay, 1980), and the Stump Formation in the Uinta Mountains of northeastern Utah (Pipiringos and Imlay, 1979; Imlay, 1980; Wilcox and Currie, 2008), reflecting the same transgressive-regressive period of the Sundance Sea (Pipiringos and O'Sullivan, 1978; McMullen and others, 2014). In the Four Corners area, the Curtis Formation has been correlated to the Todilto Member of the Wanakah Formation, whereas the Summerville Formation is replaced by the Beclabito Member of the Wanakah Formation (Condon and Huffman, 1988). Note that Anderson and Lucas (1994) used a different nomenclature for the same interval; they regarded the Todilto as a formation rather than a member, whereas the Summerville Formation extends into the Four Corners area. The Summerville Formation is capped by the J-5 unconformity (Pipiringos and O'Sullivan, 1978), which resulted from the fall of the regional base level (Caputo and Pryor, 1991; Peterson, 1994), generating a relief of at least 20 m, before being overlain by the fluvial sediments of the Tidwell Member, the lowermost unit of the continental Morrison Formation south of the Uinta Mountains (Waldschmidt and LeRoy, 1944; Peterson, 1988; Turner and Peterson, 1999). Figure 1C displays a summary stratigraphic column of the study area.

METHODS AND DATA

In order to understand the genesis of the Curtis Formation in the study area, fieldwork campaigns were conducted in 2015, 2016, and 2017. The data included in this paper comprise (1) 40 detailed sedimentary logs (figure 1), which locations were chosen based on outcrop exposure quality, accessibility, and regular distance between each measured section; (2) pictures taken at and between log-sites by all members of the research group involved in the project, as well as Unmanned Aerial Vehicles (UAVs), aerial photographs, satellite images, and open-source imagery available from Google and Microsoft Bing databases; and (3) recordings of paleocurrent directions and other structural data. Three-dimensional (3D) virtual outcrops were generated for selected localities following Westoby and others (2012) structure-from-motion photogrammetry principles, in order to assess the architecture of the sedimentary succession. UAV data were processed using PhotoScan Pro by AgiSoft (Agisoft LLC, St. Petersburg, Russia), whereas the 3D-generated models were subsequently analyzed and interpreted in Lime (developed by the Virtual Outcrop Geology (VOG) Group from the Universities of Bergen and Aberdeen). Traditional sedimentologic methods were applied, such as identification of depositional sub-environments and correlation across short and long distances in order to reconstruct the spatial and temporal distribution of sub-units of the target strata. The resultant assimilation of data allows the construction of an improved depositional model for the Curtis Formation, and sheds light on how sediments are dispersed across a shallow shelf in general.

RESULTS

Twenty-four sedimentary facies were recognized and summarized in table 1. Rock fabric, composition, and structure(s) are the key to interpreting the processes and conditions under which these sediments were deposited. As a result, these facies have been organized in eight main facies associations (FA 1 to FA 8) with six sub-facies associations (FA 1a, FA 1b, FA 3a, FA 3b, FA 4a, and FA 4b), which are summarized in table 2 and carefully described below.

These facies associations are not homogeneously distributed across the study area (figures 2 and 3). It is important to mention that the datum on which the measured sections are aligned on figure 3 corresponds to the J-3 unconformity. To increase the visibility of the correlation, 19 out of 41 visited localities were selected based on spatial distribution and completeness of the sedimentary succession. Pie charts reflect the ratio between the different facies associations present in the Curtis Formation, whereas the Entrada Sandstone and the Summerville Formation are neglected. Based on the spatial distribution of these various facies associations, it is possible to divide the study area into sectors 1, 2 and 3 (figure 3), which are discussed further below.

FA 1 – Coastal Wet Eolian Deposits

Description

This unit corresponds to the cross-stratified eolian dunes and sandy interdunes (Facies A in table 1) of the Slick Rock Member (Entrada Sandstone, FA 1a), which crops out in the eastern and southeastern part of the study area (figure 1). Towards the west, FA 1 coincides with the parallel-laminated to mottled deposits (Facies B) dominating the earthy facies (FA 1b) of the Entrada Sandstone, with interfingering trough cross-stratified sandstone (Facies C), rippled cross-stratified sandstone (Facies U), and isolated coastal eolian dunes (Facies A). The hoodoos of Goblin Valley State Park mainly consist of structureless sandstone (Facies D). This sedimentary package thickens westward. Only at Safari Road (figure 1), FA 1 is capped by a rusty-red, calcite-cemented, thoroughly bioturbated, fine-grained sandstone (Facies E). Facies C (trough cross-stratified sandstone) occurs sporadically within FA 1, reaching a maximum thickness of about 1 m and is located 13 m below the base of the Curtis Formation at the Crystal Geyser section (figure 1). Here, the well-sorted foresets alternate between coarse and fine-grained sand with potential double mud drapes. Facies A, Facies B, Facies C, and Facies T are characterized by a sharp contact at their base, which can also be erosive, especially for Facies A, C, and T. Facies T usually appears both at the base and at the top of eolian dune packages (Facies A) but can also crop out

Table 1. Facies description for the Entrada Sandstone, Curtis Formation, and Summerville Formation (continued on following page).

Facies	Description	Structures	Grain Size*	Interpretation	Formation
A	Cross-stratified sandstone	Unidirectional tangential cross-bedded very fine to fine-grained sandstone, alternating grain flow and grain fall deposits, sharp base, rusty red or white, locally bleached, local occurrence of rhizoliths, varying bedform/bedform sets size, maximum individual dune thickness 15 m. Potential occurrence of counter-ripples at the toe of the foresets	VF - F	Eolian dune deposits, locally influenced by a dynamic and migrating water table/saturated level	Entrada Ss. Moab Mbr.
B	Plane parallel-laminated to mottled mudstone with localized evaporites	Dark red silty mudstone with pale yellow to white very fine to fine-grained sand lenses, plane parallel-laminated to -stratified or mottled, potential bleached patches around rhizoliths, localized evaporite-rich horizons, maximum individual horizon 1 cm	Si - Cl	Eolian interdune deposits showing occasional flooding with development of sabkha-type deposits and/or superficial vegetation	Entrada Ss. Summerville Fm.
C	Trough cross-stratified sandstone	Trough cross-stratified very fine to medium-grained sandstone, potential mud drapes and rip-up mud clasts, eventual desiccation cracks and/or evaporite-rich horizons. Thickness ranging between dm- to m values	VF - M	Tidally influenced migrating 3D-dunes	Entrada Fm. Curtis Fm. Summerville Fm.
D	Structureless fluidized sandstone	Deformed to structureless fluidized of green to pink silt to fine-grained sandstone, local fluid-escape and loading structures still visible, sometimes visually expressed as well rounded sandstone boulders with injected mudstone, maximum boulder diameter (Ø) 25 cm, maximum bed thickness 2 m	Si-F	Destruction of original sedimentary structures due to fluids flowing through the sandstone bed or through liquefaction of water-saturated horizons	Entrada Ss. Curtis Fm.
E	Thoroughly bioturbated condensed sandstone	Rusty-red condensed, cemented, fine-grained sandstone, thoroughly bioturbated., maximum thickness 25 cm	F	Sediment starvation in a semi-arid coastal plain setting	Entrada Ss.
F	Matrix-supported basal conglomerate	Rounded to well-rounded, matrix-supported basal conglomerate, no preferred clast orientation but their long axis tend to be parallel to the bedding plane, matrix consists of fine- to medium-grained sandstone, maximum clast Ø 8 cm, maximum bed thickness 20 cm	F-Pb	Flash flood deposits	Curtis Fm. ?
G	Planar- to low angle cross-stratified sandstone	Plane-parallel to low-angle cross-stratified, very fine to fine-grained, gray to green to white sandstone, potential herringbone cross-lamination, current and oscillation ripple-lamination, as well as dm-scale soft-sediment deformation, maximum individual bed thickness 60 cm	VF - F	Upper shoreface to beach deposits with tidal influence	Curtis Fm.
H	Tangential cross-stratified gravelly sandstone	Matrix-supported conglomeratic dune, hm-scale lateral extent, sub-horizontal erosive base, rip-up mud clasts, extra-basinal sub- to rounded clasts, maximum clast Ø 2.5 cm, unidirectional current trough cross-stratification, maximum individual dune thickness 2.5 m	M - Gr	High energy, asymmetric tidal flow pattern within a laterally restricted embayment	Curtis Fm.
I	Tidally influenced cross-stratified conglomeratic sandstone	Matrix- to clast-supported lense-shaped intraformational conglomerate of restricted lateral extent, locally developed and amalgamated in tidal bundles, rip-up mud clasts, extra-basinal sub- to rounded clasts, maximum clast Ø 2.5 cm, bidirectional cross-stratification with superimposed current ripples, maximum bed thickness 60 cm	F - Gr	High-energy tidal channels–inlets	Curtis Fm.
J	Planar cross-stratified sandy conglomerate	Clast- to matrix-supported conglomerate, hm-scale lateral extent, convex-down erosive base, flat top, extra-basinal sub- to rounded clasts, maximum clast Ø 2.5 cm, planar cross-stratification, maximum individual thickness 3.0 m	M - Gr	Point bar lateral accretion within a migrating tidal channel	Curtis Fm.
K	Plane parallel-laminated mud- to siltstone	Plane parallel-laminated mud to siltstone, scattered bidirectional current ripple cross-stratifications, gray to green, occasional desiccation cracks, sporadic bioturbations both parallel and normal to the bedding planes	Si - Cl	Gentle flow activity with tidally related current reversals	Curtis Fm.

*Cl=clay, Si=silt, VF=very fine, F=fine, M=medium, Gr=gravel, Pb=pebble; Grain size in parenthese denotes rarely present and bracketed denotes at the boundary betwen VF and F

Table 1 (continued from previous page). Facies description for the Entrada Sandstone, Curtis Formation, and Summerville Formation.

Facies	Description	Structures	Grain Size*	Interpretation	Formation
L	Heterolithic silt- and sandstone with lenticular bedding	Rippled very fine to fine-grained sandstone, grayish lenses containing herringbone and current ripple cross-stratifications within a matrix of laminated gray to green mud- to siltstones, occasional desiccation cracks, sporadic bioturbations both parallel and normal to the bedding planes	Si - F	Current reversals in lower subtidal zone	Curtis Fm.
M	Heterolithic silt- and sandstone with wavy bedding	Ripple cross-stratified very fine to fine-grained grayish sand layers, with bi-directional current indicators and interbedded with laminated gray to green siltstone, occasional desiccation cracks, sporadic bioturbations both parallel and normal to the bedding planes, varying amount of organic matter	Si - F	Current reversals in subtidal zone (shallower than Facies L)	Curtis Fm. Moab Mbr.
N	Heterolithic sandstone with flaser bedding	Ripple and herringbone cross-stratified very fine to fine-grained gray to green to white sandstone, scattered mud lenses, as well as single and double mud drapes, varying amount of organic matter	VF - F	Upper sub- to lower intertidal sandy flat	Curtis Fm.
O	Sandstone with climbing ripples	Climbing ripple cross-stratified very fine to fine-grained sandstone, gray to green	VF - F	Tidal channel overbank spill on tidal flat, Upper sub- to lower intertidal sandy flat	Curtis Fm.
P	Cross-stratified sandstone arranged in well-defined rhythmic tidal bundles	Very fine to fine-grained (medium-grained rarely present) gray to green to white sandstone, arranged in tidal bundles, with occasional anti-ripples documented from their toesets, varying amount of organic matter	VF - F (-M)	Tidal inlets, lower energy than Facies I	Curtis Fm.
Q	Structureless sandstone	Very fine to fine-grained grained gray to green to white sandstone, massive, with potential scattered single and-or double mud drapes. Usually rounded and smoothly weathered	VF - F	The nature of the lack of structure might only be due to intensive surface weathering. Presence of mud drapes indicate sub- or intertidal environment	Curtis Fm.
R	Thoroughly bi-directional rippled cross-stratified sandstone	Thoroughly rippled silt to very fine grained sandstone, dominated by herringbone cross-stratifications	S - VF	Deep subtidal environment with near equal flood and ebb tidal current conditions. Note that the weathering can in some cases erase most of the sedimentary structures	Curtis Fm. Moab Mbr.
S	Plane parallel-stratified sandstone	Plane parallel-stratified very fine to fine-grained sandstone with scattered current ripple lamination, white, pink or green. Note that the weathering expression of this facies varies between the different units of the Curtis Fm. Potential mud cracks and soft-sediment deformation	(Si-) VF - F	Sandy tidal flat, upper flow regime (to lower antidune-regime?). Documented mud cracks indicate short-lived subaerial exposure	Curtis Fm. Moab Mbr.
T	Condensed sandstone	Thin, yellow structureless sandstone, occasionally displaying low-amplitude undulations, exclusively observed capping the Moab Member of the Curtis Fm. Maximum bed thickness 10 cm	[VF-F] F	Condensed horizon	Moab Mbr.
U	Rippled cross-stratified sandstone	Undulated to rippled cross-stratified, very fine to fine-grained, gray to brown sandstone, with 3D current ripples, possible interference ripples, potential mud cracks and soft-sediment deformation	VF - F	3D migrating ripples under unidirectional current conditions	Entrada Ss. Curtis Fm. Moab Mbr. Summerville Fm.
V	Plane parallel-laminated siltstone	Dark red soft slope-forming siltstone, most probably plane parallel-laminated, scattered pale white bleached lenses and evaporites	Si	Supratidal plain	Summerville Fm.
W	Iron rich ripple- and parallel-laminated sandstone	Dark red to brown cemented very fine to fine-grained sandstone, gentle ripple cross-stratification, potential desiccation cracks	VF - F	Fluvial overbank flooding deposits	Summerville Fm.
X	Paleosol	Dark purple mud or silt	Cl-Si	Sub-aerially exposed surface with superficial soil development	Entrada Ss. Curtis Fm. Moab Mbr. Summerville Fm.

*Cl=clay, Si=silt, VF=very fine, F=fine, M=medium, Gr=gravel, Pb=pebble; Grain size in parenthese denotes rarely present and bracketed denotes at the boundary betwen VF and F

Table 2. Facies associations for the Entrada Sandstone, Curtis Formation, and Summerville Formation.

Facies Association	Depositional Environment	Facies Included	Formation
FA 1a	Coastal wet eolian dune system (Kocurek and Havholm, 1993; Mountney, 2012), with episodic (marine) partial flooding of interdunes deposits and superficial development of soil- and vegetated horizons	A, C, X	Entrada Ss. Slick Rock Mbr.
FA 1b	Coastal wet eolian interdune system (Kocurek and Havholm, 1993; Mountney, 2012), with episodic (marine) partial flooding of interdune deposits and superficial development of soil and vegetated horizons	B, C, D, X	Entrada Ss. earthy facies
FA 2	Beach deposits to upper shoreface deposits, with potential associated tidal channel cut-and-fill	C, G, S, U	Curtis Fm.
FA 3a	Subtidal heterolithic mud, silt, and very fine grained sandstone, generally coarsening up from laminated mudstone, wavy bedding, scarsely bioturbated	H, I, J, K, L, M	Curtis Fm.
FA 3b	Subtidal heterolithic vf- to f-grained sandstone generally coarsening up from wavy bedding to flaser bedding, scarsely bioturbated	H, I, M, N	Curtis Fm.
FA 4a	Sandy tidal flat with correlative major tidal channels, having potential subaerial exposures	S, U, X	Curtis Fm.
FA 4b	Tidal channel infills and splays, distal correlative of FA 4a in the northern areas	C, H, I, L, M, N, S, U	Curtis Fm.
FA 5	High energy, sub- to intertidal sand -dominated environments, encompassing tidal flats, tidal channels, and beaches	C, G, (K, L, M,) N, O, P, Q, R, S(, X)	Curtis Fm.
FA 6	Upper intertidal heterolithic channels and flats complex, fining up, with intermittent prolonged subaerial exposures and rare bioturbation, indicator of a more stressed environment than FA 3	K, L, M, N, Q, S, U, X	Curtis Fm.
FA 7	Coastal dry eolian dune field (Mountney, 2012), arranged in four to five sequences separated by supersurfaces, upon which transgressive water-carried sediments and/or paleosol can be observed	A, N, Q, S, T, U, X	Curtis Fm. Moab Mbr.
FA 8	Supratidal lower coastal plain, with episodic marine flooding	U, V, W, X	Summerville Fm.

as individual beds within a mottled interval (Facies B). Note that Facies B can locally grade up-section into paleosols (Facies X). Bleached patches of rock commonly underlie and overlie paleosols or are found in the direct vicinity of such horizons, contributing to the mottled expression (Blodgett, 1988). The top of FA 1 is capped by regional J-3 unconformity of Pipiringos and O'Sullivan (1978).

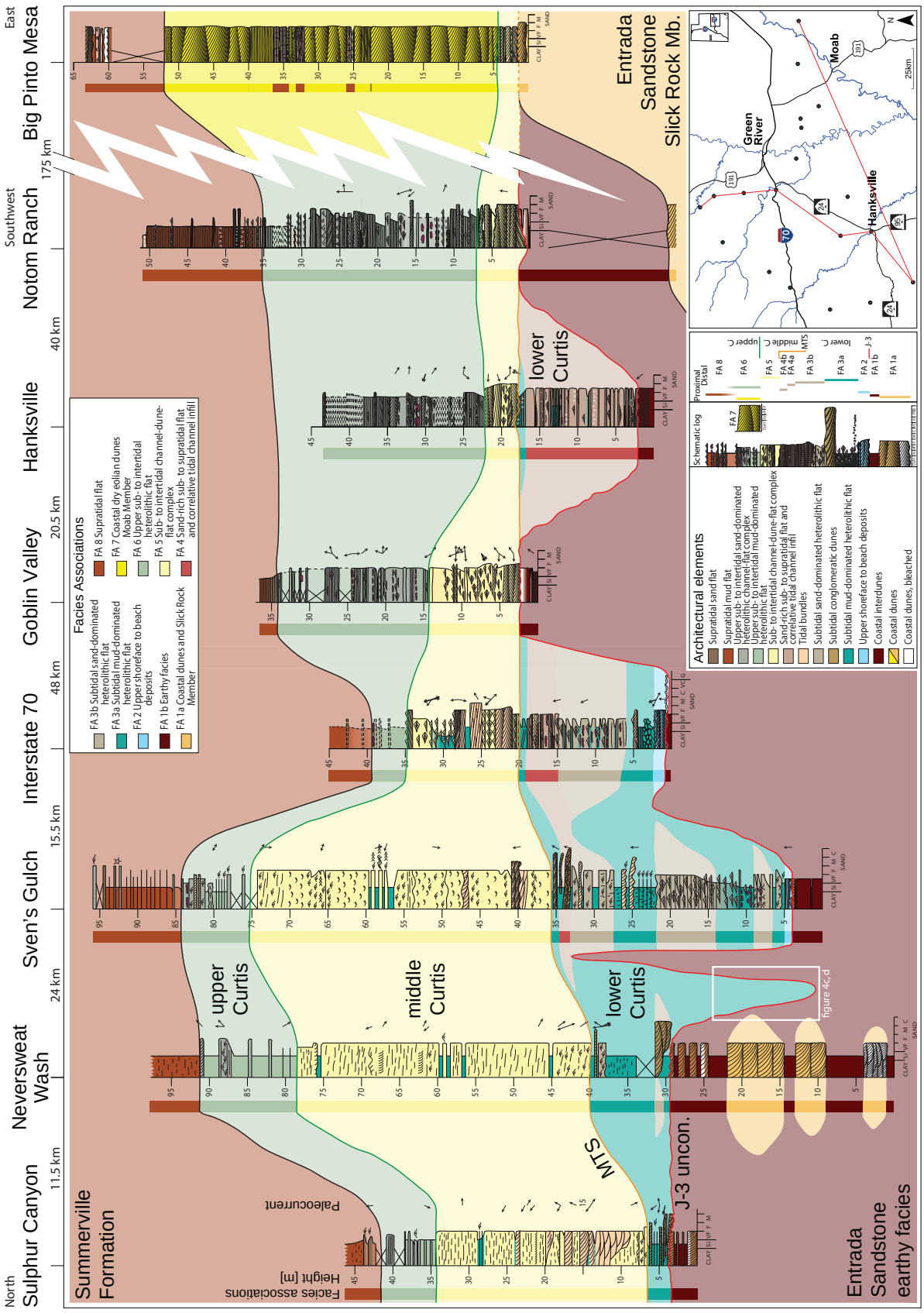

Figure 2. North-southwest-east cross section across the study area showing the spatial distribution of the main facies associations identified within the uppermost strata of the Entrada Sandstone, the Curtis Formation and the lowermost strata of the Summerville Formation along the western margin of the San Rafael Swell and south to the Henry Mountains. The Big Pinto Mesa measured section represents the typical expression of the Moab Member of the Curtis Formation. Detailed sedimentary information on the various architectural elements present at the selected localities is displayed on the measured sections, whereas facies associations are color-coded in each summary column next to their respective measured section.

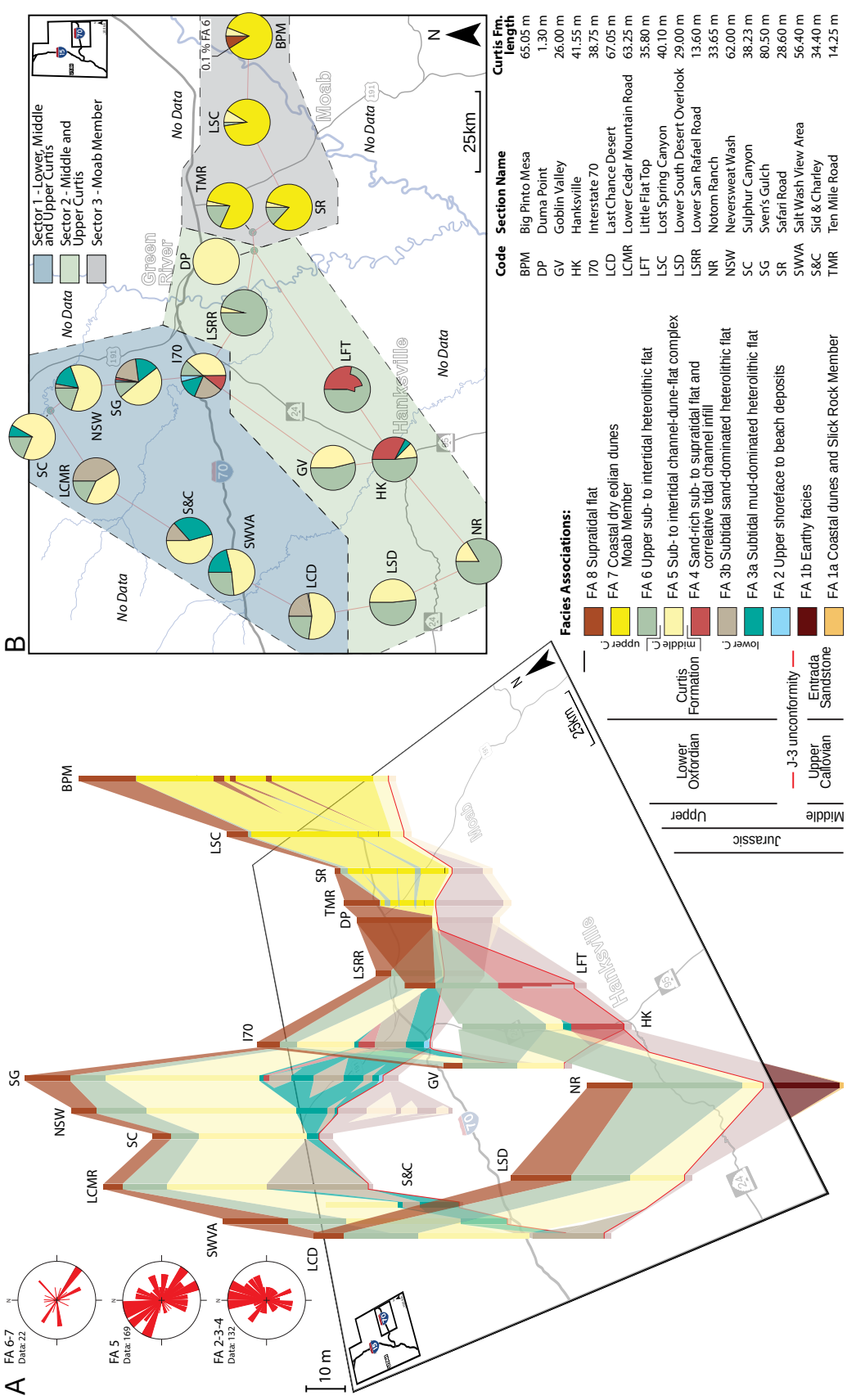

Figure 3. (A) 3D correlation between selected localities. As the sedimentary sections are aligned on the J-3 unconformity (red line), the Entrada Sandstone appears below the map, whereas the Curtis Formation remains above it. Paleocurrent measurements are arranged stratigraphically from bottom to top. (B) Pie charts representing the ratio between the different facies associations belonging to the Curtis Formation at each localities. See text for discussion of unusual pattern in Little Flat Top (LFT).

On a structural geology note, numerous conjugated extensional faults, associated fractures, and remobilized, injected and disintegrated sand (Facies D), as well as hydroplastic deformation occur in the upper Entrada Sandstone in the Humbug Flats area, at Smith's Cabin in the north, farther south between Interstate 70 and Uneva Mine Canyon, and north of Hanksville Airport (figure 1). Fractures typically feature a bleached front in their direct vicinity (figure 4A). Fault planes are mostly planar; however, growth-fault geometry on south-facing faults is found near Smith's Cabin. Faults show meter-scale offset in the earthy facies of the Entrada Sandstone, whereas most of them are concealed by the base of the Curtis Formation, which remains undisturbed. Faults strike east-west around the Humbug Flats-Smith's Cabin area in the north; whereas south of Interstate 70 they strike north-south. Note that bleaching is common along fractures and faults within FA 1 (figure 4a). However, 2.1 km north of Hanksville Airport, the earthy facies (FA 1b), was impacted by syn- to post-depositional localized extensional and contractional faults, as well as synchronous erosion, generating a 2 to 3 m relief at the top of the Entrada Sandstone (figure 4F). These fault clusters display a semi-circular surface expression. The heterolithic deposits of lower Curtis (FA 3-4) passively filled the preexisting topography, before being rapidly overlain by the middle Curtis sediments (FA 5), which abruptly collapsed by faulting while or shortly after being deposited. It remains unclear how precisely and when these processes jolted the deposits of the middle Curtis.

Interpretation

Interbedding of eolian dune, interdune, sabkha, and tidal deposits are typical features for coastal wet eolian desert environments, as interpreted and described by several authors (Crabaugh and Kocurek, 1993; Kocurek and Havholm, 1993; Mountney, 2012). Occurrence of marginal marine sandstones, gypsum-rich beds, and paleosols horizons within an interval dominated by Facies B are related to partial marine flooding and/or relative water table rises within the sediments (Carr-Crabaugh and Kocurek, 1998; Mountney, 2006). On the contrary, intervals dominated by eolian dunes reflect short-lived relative base level falls (Mountney, 2006, 2012). Mottling is ascribed to forced disturbance from roots and has been enhanced by circulation of organic acids through the tight mudstones (Blodgett, 1988), most probably flowing along root burrows. Also, the development of the condensed and bioturbated sandstone bed (Facies E) at the top of FA 1 indicates an extended period of sediment starvation (Urash and Savrda, 2017) around the area known today as Safari Road (figure 1). Consequently, FA 1 is considered to represent a coastal eolian system, where marine processes and water table variations jointly and increasingly influenced the sedimentary development of the Entrada Sandstone. Bleached fronts observed along fractures in the earthy facies occurred as a consequence of post-depositional reducing fluid circulation within a naturally CO_2-charged system (Kampman and others, 2013; Ogata and others, 2014; Skurtveit and others, 2017; Sundal and others, 2017). As conjugated fault sets mostly offset the strata of the earthy facies, consequent extensional faulting appears to have occurred post-earthy facies deposition, but pre-Curtis sea transgression. The occurrence of disturbed earthy facies layers, as well as lower and middle Curtis strata 2.1 km north of Hanksville Airport implies that the lowermost Late Jurassic strata responded to episodes of sand mobility which impacted the surface morphology.

FA 2 – Beach to Upper Shoreface Deposits

Description

FA 2 is recorded at Curtis Point, Sven's Gulch, Interstate 70, and Uneva Mine Canyon measured sections (figure 1). It reaches a maximum thickness of about 1.70 m at Sven's Gulch. FA 2 shows a clear upward-fining trend, where the lowermost plane parallel-stratified sandstone of Facies S and planar to low-angle cross-stratified sandstone of Facies G are overlain by the trough cross-stratified sandstone of Facies C and/or ripple-laminated sandstone of Facies U. Mud drapes and rip-up clasts are also documented at Interstate 70 and Uneva Mine Canyon. FA 2 overlies FA 1, from which it is separated by the J-3 unconformity, locally displaying load structures (figure 5). The transition between FA 2 and the overlying FA 3 occurs either as a gradual and

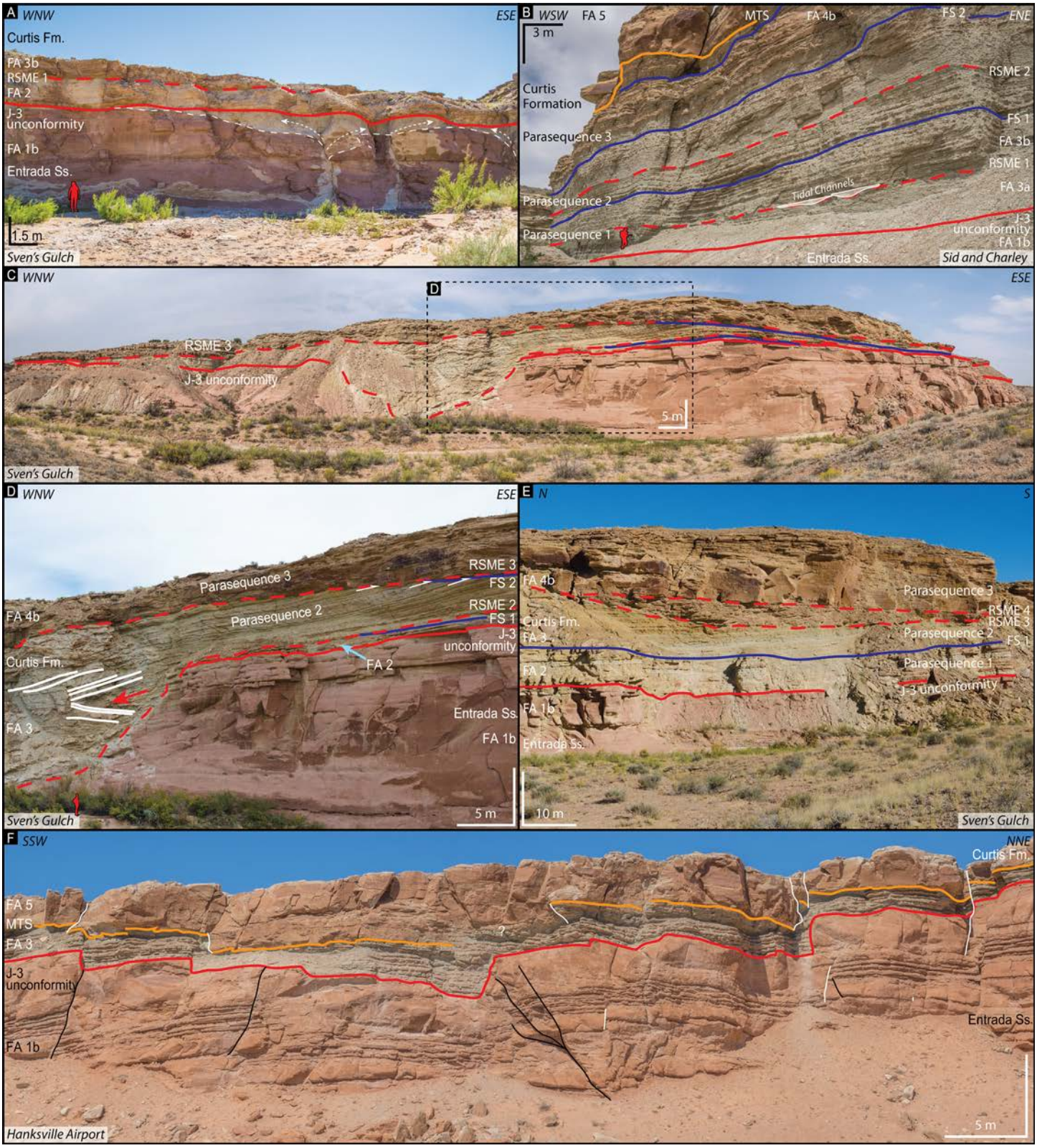

Figure 4. Caption on the following page.

Figure 4 (figure on the previous page). Overview of the lower Curtis in sector 1. See figure 3 for sectors, and figure 1 for photograph locations. (A) The beach to upper shoreface deposits of FA 2 overlie the earthy facies of Entrada Sandstone (FA 1b) at Sven's Gulch. FA 2 is truncated at its top by a Regressive Surface a Marine Erosion (RSME), corresponding to the base of FA 3b (Sand-Dominated Subtidal Heterolithic Flat). Note the plume geometry of the bleached zones below the J-3 unconformity, suggesting a trapping of the reducing fluids below the sand of FA 2 as they circulate along fractures within the Entrada Sandstone (white arrows; Skurtveit and others, 2017, Sundal and others, 2017). (B) The three parasequences occurring in the lower Curtis, as observed at the Sid and Charley sections on the western margin of the San Rafael Swell. Note the occurrence of two small tidal channels (white surfaces) at the base of RSME 1 (FS: Flooding Surface). The lower Curtis is capped the a Major Transgressive Surface (MTS), which can be traced across the study area. (C and D). Major tidal incision observed at Sven's Gulch, carved during a short-lived regressive phase within Parasequence 2. The red arrow points at a boulder of Entrada Sandstone within a matrix of Curtis Formation, indicating that the Entrada was poorly lithified when incised. The presence of this boulder, as well as FA 3 cannibalising its substratum, show that this depression was actually carved into the Entrada Sandstone by tidal currents, rather than being a pre-existing relief subsequently filled by the Curtis Formation. Note also the bi-truncation of Parasequence 2 during the early transgression of Parasequence 3, followed by the cannibalisation by FA 4b of its substratum during a short-lived regressive phase within Parasequence 3. (E) Display of two incision phases within the FA 4b deposits of Parasequence 3. (F) Collapse structure complex linked to sand mobility in the lower and middle Curtis cropping out 2.1 km north of Hanksville Airport. White lines indicate normal faults, whereas the black lines highlight contractional structures.

fining-upward changeover or corresponds to a sharp and erosive contact (figures 4a and 5). Note that the lateral extent of FA 2 reaches 200 to 500 m, and at the measured section Interstate 70, FA 2 is arranged in laterally accreting sandstone bodies, interbedded with FA 3 finer heterolithic material.

Interpretation

The high sand content of these rocks combined with the extremely low mud content indicate a high-energy marine environment. The deformation of the J-3 unconformity and the underlying FA 1b by loading suggests a poorly lithified Entrada Sandstone at the time of deposition (Owen and others, 2011). The occurrence of oscillation ripple lamination, as well as planar to low-angle cross-stratified sedimentary structures are clear indicators of upper shoreface to beach deposits. The occurrence of rip-up clasts and mud drapes testifies of secondary tidal action over the system. The overall fining-upward trend from FA 2 into FA 3 indicates a gradual transgression of the Curtis sea over the J-3 unconformity, whereas the restricted character of FA 2 suggests a direct influence of the pre-existing erosional relief over the distribution of these marginal marine deposits. They represent the onset of marine deposition into an erosional topography, and thus initially filled the available accommodation in the dips and furrows. FA 2 also displays the same deepening-upward development at Sven's Gulch. However, its base is characterized by a short-lived shallowing-upward event, as recorded by the basal oscillation ripple-laminated sandstone of Facies U (ripple-laminated sandstone). It is then overlain by the 3D migrating dunes of Facies C before grading into the high-energy deposits of Facies S (plane-parallel stratified sandstone) and G (planar to low-angle cross-stratified sandstone). It subsequently follows the same deepening-upward pattern as mentioned above. The fact that these marginal marine-beach deposits are only documented from the measured sections south of Curtis Point (figure 1) suggests a flooding of the southern areas from the northeast, before expanding towards the northern higher grounds.

FA 3 – Heterolithic Subtidal Flat and FA 4 – Sand-Rich Sub- to Supratidal Flat and Correlative Tidal Channel Infill

Description

FA 3 (figure 4) displays the lowermost sedimentary package, which represents the Gilluly and Reeside (1928) type section of the Curtis Formation and crops out mostly in sector 1, as well as Little Flat Top and Hanksville (figure 3). It is separated into a lower mud-dominated interval (FA 3a), which grades into an

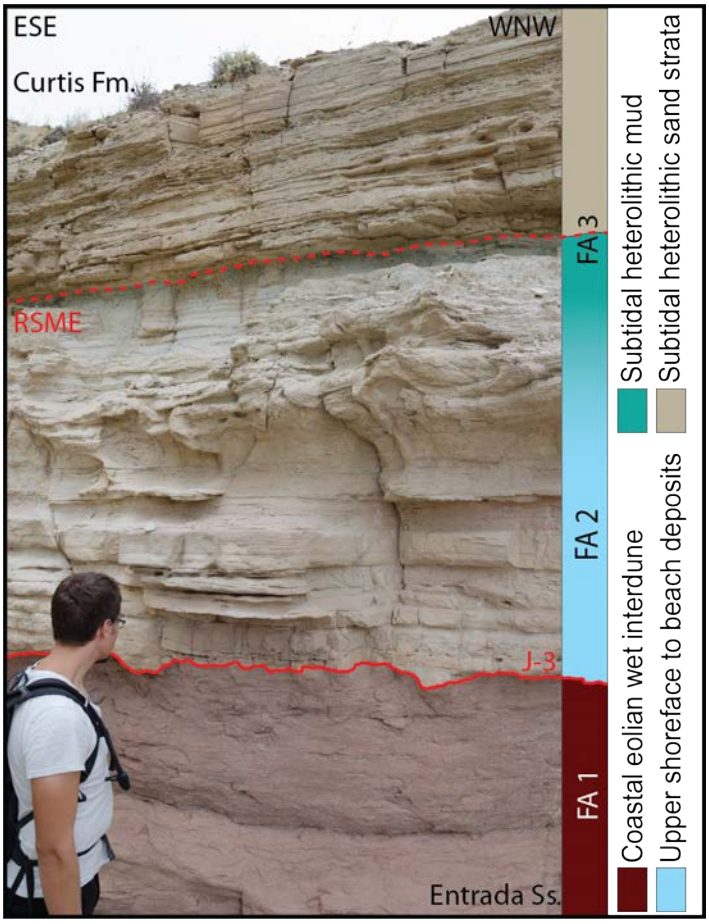

Figure 5. Transition from the Entrada Sandstone into the lower Curtis as observed at Sven's Gulch. FA 2 (beach to upper shoreface deposits) overlies the earthy facies of the Entrada Sandstone (FA 1b), from which it is separated by the J-3 unconformity. Note the presence of load casts at the base of FA 2 at some localities. FA 2 rapidly grades into FA 3a (mud-dominated heterolithic subtidal flat), which can be cannibalised by the sand-dominated subtidal deposits of FA 3b (RSME: Regressive Surface of Marine Erosion).

upper sand-dominated association (FA 3b) (table 2). FA 3a and FA 3b dark-green to gray color makes it readily identifiable in the field, where their combined thickness can vary significantly over a few hundred meters, ranging from less than a meter to about 30 m. FA 3 (dis)conformably overlies or onlaps the J-3 unconformity which caps FA 1 notably in the northern part of the study area (figure 1). It can also overlie FA 2 from which it fines upward or erodes into (figures 4 and 5). FA 3 displays at least two major coarsening-upward parasequences (Parasequence 2 and Parasequence 3) (sensu Catuneanu and others, 2009). A third parasequence (Parasequence 1) has been observed at Sven's Gulch and the Sid and Charley section (figure 1). Both Parasequence 2 and Parasequence 3 comprise a suite of sedimentary facies commonly associated with tidal deposits: FA 3a includes laminated mudstone (Facies K), lenticular (Facies L), and wavy bedding (Facies M), whereas FA 3b comprises wavy bedding (Facies M) and flaser bedding (Facies N), with the presence of straight, sinuous-crested, and linguoid current ripples, as well as herringbone cross-lamination. Sub-vertical and sub-horizontal bioturbations are recorded in FA 3a and FA 3b; the degree of disturbance varies, but remains limited, and corresponds to Droser and Bottjer's (1986) ichnofabric index n°3. Furthermore, their diversity is circumscribed to only a few types, such as *Thalassinoides*, *Cruziana*, or *Gyrochorte comosa* ichnofossils, similarly reported from the Carmel Formation (De Gibert and Ekdale, 1999). FA 3 increases in grain size towards the south, with a generally higher sand-to-mud ratio on the western margin of the study area. Its upper boundary is truncated by FA 5, which can, however, be locally conformable.

A significant tidal incision can be observed at Sven's Gulch, carving about 15 m into its substratum (FA 1b and FA 2) and reaching a width of about 60 m (figures 4C and 4D). The infill of that incision shows an intricate architecture, which mostly consists of FA 3b material, as well as one boulder of earthy facies (FA 1b). Meter-scale, runnel-shaped gravelly bodies (Facies I) are also documented at all locations north of Sven's Gulch, displaying evidence of tidal reworking within a heterolithic environment. The area north of Middle Canyon (figure 1) is marked by the occurrence of laterally extensive gravel-rich compound dunes, displaying basinward-dipping, meter-thick tangential cross-stratification, with a non-erosive bedding-parallel base and a concave-up top surface (Facies H) (figure 6), and are usually found in the lowermost meters of the Curtis Formation. Conglomeratic dunes are not to be mistaken with the laterally accreting conglomeratic tidal channels, which are characterized by planar to tangential cross-stratification and a concave-down erosive base (Facies I and J). Also, at the measured section just south of Interstate 70, FA 2 is overlain by a 1-m-thick greenish-colored sandstone,

Figure 6. (A) Outline of a westward laterally migrating tidal channel observed in the cliffs of Cedar Mountain, filled by the conglomeratic sandstone of Facies I. The transition from a cross-stratified conglomerate into a more parallel-bedded conglomerate reflects a change in the channel orientation, as the cross-stratified deposits correspond to a transversal cross section of the channel, whereas the parallel-bedded part of the channel represents a longitudinal cross section through the same channel. (B) Transversal section across a north-westward migrating conglomeratic dune (Facies H, table 1) in the cliffs of Last Chance Desert. This dune was influenced by tidal processes, as illustrated by the bundle-like regular and rhythmic thickness variations observed between the foresets. The biggest discrepancy between the tidal channel and the tidal dune resides within their respective base. The tidal channel displays a concave-down erosive base and a flat upper surface, whereas the dune is characterised by a non-erosive and bedding-parallel base and a convex upper boundary.

completely disturbed by processes related to liquefaction and water escape (Facies D), which has not been observed anywhere else in the study area. The road cut section measured at Last Chance Desert (figure 1) also displays a unique feature which has not been documented anywhere else: a 20-cm-thick, matrix-supported basal conglomerate, with randomly oriented, rounded to well-rounded extra-basinal clasts that are about 8 cm in diameter (Facies F). The outcrop exposure of this conglomeratic bed limits the exact measurement of its lateral extent, but reaches a minimum of 70 m.

FA 4a conformably lies within and must interfinger with FA 3a and FA 3b within Parasequence 2. It represents 30% to 50% of the Curtis Formation in Hanksville and Little Flat Top, but it has not been observed at the locations north of Smith's Cabin nor on the western margin of the San Rafael Swell (figures 1, 2, 3, and 7). It is characterized by its dominant light-pink, plane parallel-stratified or structureless, very fine to fine-grained sandstone (Facies S) and subordinate unidirectional straight-crested 2D and 3D current ripple-dominated intervals (Facies U), as well as centimeter-thick marine mudstone. Episodes of subaerial exposure are recorded as dark-purple paleosol horizons (Facies X, figure 7) or desiccation cracks. Each individual bed measures as much as 1.50 m thick and can be laterally traced over several kilometers. Although appearing isopachous at outcrop scale, its thickness ranges from about 15 m at Rabbit Gulch to 2 m at Uneva Mine Canyon (figure 1), and it reaches a maximum of about 20 m thick at Little Flat Top (figure 1). About 250 m south of the Interstate 70 measured section, FA 4a forms a convex-down, flat-topped feature with sand-dominated heterolithic beds that thicken towards the center. It measures 6.25 m thick and about 45 m wide. At first glance, the architecture and shape resemble a channel infill succession, but it lacks any erosional scour at its base or internally. It only thickens in its central part due to differential loading (figure 7D). FA 4b has exclusively been documented in the Parasequence 3 interval at Sven's Gulch (figure 1), where the measured section traces a 15 m thick succession between two tidal channels that incise their FA 3 substratum by as much as about 10 m (figures 4C, 4D, and 4E). Note that at least two episodes of incision might have occurred during the deposition of FA 4b, as visible in Sven's Gulch. The first incision carves the deepest into the FA 3a-3b deposits, whereas the second incision is shallower. The channel infills are dominated by Facies H, I, N, C, S, and U, with a very high sand-to-mud ratio. No evidence of subaerial exposure is recorded in FA 4b. The channel margins contain Facies H and Facies I, which interfinger with Facies E, F, M, P, and Q. Individual beds are >1 m thick. FA 2, FA 3, and FA 4 are dominated by a north to north-northeast paleocurrent direction, with some northeast flows and with a subordinate and opposing south-southwest component (figure 3). Note the strong underrepresentation of west-southwest to southwest flow indicators (figure 3).

Interpretation

The heterolithic nature of FA 3 indicates a fluctuating energy level within the system (Kvale, 2012). Straight-crested to linguoid ripple marks suggest different durations of flow events, as equilibrium linguoid morphology requires more time to form (Baas, 1999). The presence of Parasequence 0 exclusively at Sven's Gulch suggests that this area was the first part of the system to be flooded. The base of each parasequence is marked by a flooding surface and the development of FA 3a, followed by the coarsening-upward tidally influenced sediments of FA 3b. This is envisioned as a result of increased energy within the system due to shallower water and an increasingly proximal subtidal to tidal flat setting. The same increased energy trend is also indicated by the coarsening southward of FA 3, which suggests shallower water depth towards the present-day location of Hanksville. Whereas several flooding surfaces may be identified in outcrops, their exact correlation between the different measured sections is impossible due to the extreme dynamic nature of tidal environments, and because these flooding surfaces might stem from local variations in relative sea level such as avulsions, rather than regional signals.

When traced laterally, the infill of the steep and deep incision observed at Sven's Gulch (figures 4C and 4D) belongs to Parasequence 2. The occurrence of an Entrada Sandstone boulder within a matrix of Curtis Formation indicates that the Entrada Sandstone was

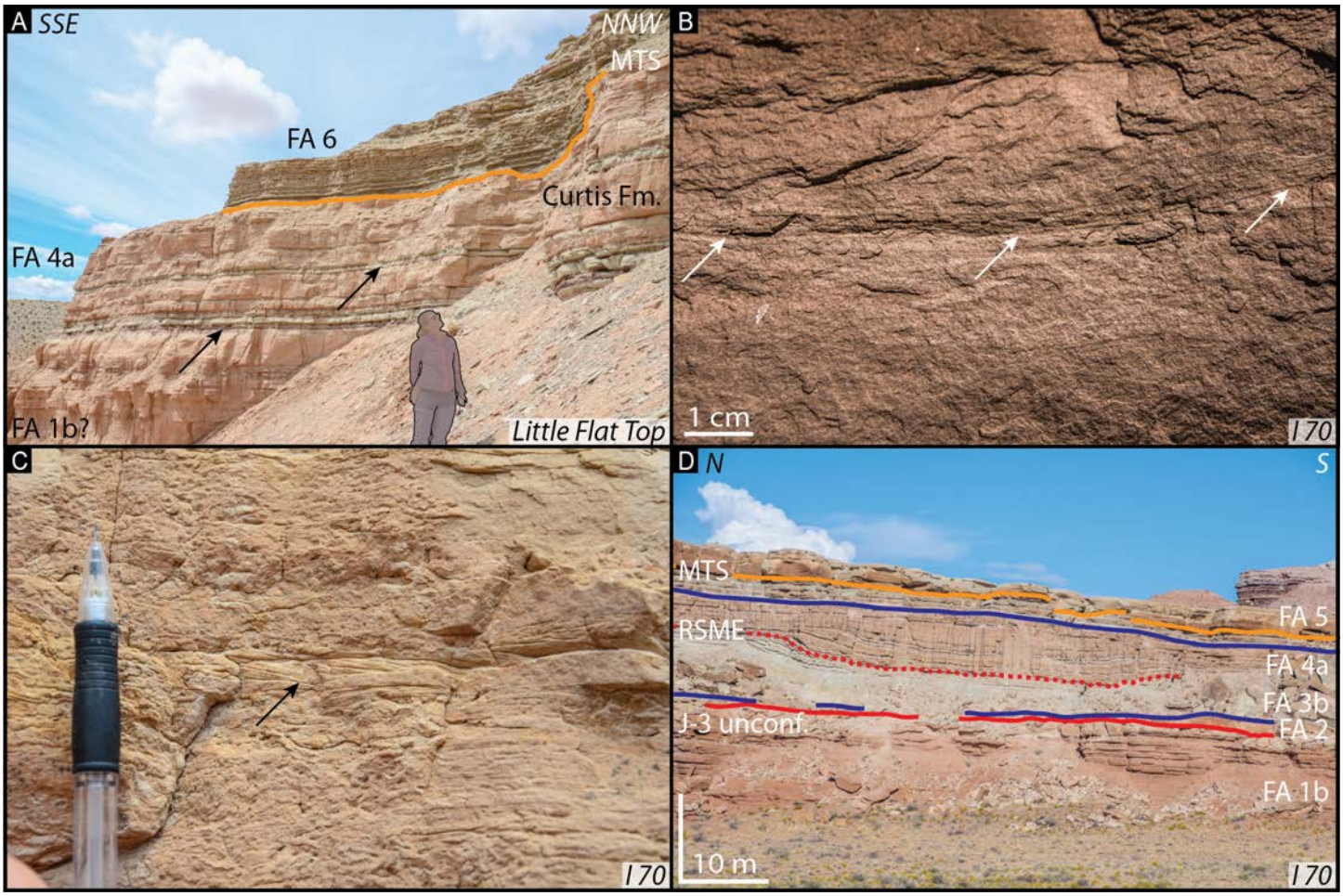

Figure 7. Overview of FA 4a. (A) Picture of Little Flat Top, where the light pink, isopachous sand-rich sub- to supratidal flat deposits of FA 4a overlie the earthy facies of the Entrada Sandstone (FA 1b). The exact location of the J-3 unconformity at that location remains uncertain due to the lack of an erosive, or flooding surface between these two facies associations, uncertainty reinforced by an unusual gradual color change between FA 1b and FA 4a. The black arrows indicate paleosol horizons which could potentially represent the lithostratigraphical boundary between the two formations. FA 4a is capped by the Major Transgressive Surface (MTS), and subsequently overlain by the sub- to intertidal deposits of FA 6, whereas the FA 5 is absent. (B) Double mud drape indicated by the white arrows, suggesting occasional subtidal depositional conditions. (C) Scattered unidirectional current ripple within a fine-grained sandstone dominated by upper-flow regime plane parallel-stratifications, which, together with the near-lack of clay material, suggest higher energy conditions in FA 4a with respect to FA 3. (D) Mini sag basin formed by the collapse of FA 3b deposits while being filled by the sandstone of FA 4a, just south of Interstate 70, near where the highway cuts through the eastern flank of the San Rafael Swell.

poorly lithified as the tidal currents funneled into it, highlighting the poly-nature of the J-3 unconformity. Both the presence of this boulder and a FA 3 cannibalizing its substratum show that this depression was actually carved into the Entrada Sandstone by tidal currents during a short-lived regressive phase within Parasequence 2, rather being a pre-existing negative relief subsequently and passively filled by the Curtis Formation.

The limited bioturbation degree and diversity indicate stressed environmental conditions within a restricted, tidally influenced marginal-marine tidal flat setting, potentially indicating hypoxic conditions as well as salinity values superior to normal marine standards (Middleton, 1991; Nio and Yang, 1991; De Gibert and

Ekdale, 1999; Fan, 2012; Hughes, 2012; Daidu, 2013). The laterally extensive compound conglomeratic dunes of Facies H in the northern area require high energy within the system at time of deposition. This succession shows strong similarities with the modern submarine dune field in laterally restricted San Francisco Bay, especially regarding the protracted extent of these features and their unidirectional, basinward development, suggesting a dominant ebb tide and subordinate flood tide as advocated by Barnard and others (2006). These conglomeratic dunes coexist with laterally migrating tidal channels (Facies J). The occurrence of cross-stratified conglomeratic lenses with interfingered greenish-colored silt and mud implies significant variation and asymmetry in current velocities, at least locally. The dominant current will mobilize gravel and coarse sand, forming lens-shaped dunes, locally amalgamated within a tidal channel, whereas the subordinate current will cut the bedform, generating reactivation surfaces, and potentially develop counter ripples and small dunes.

The replacement of the greenish-colored tidally influenced deposits of FA 3 by the pinkish-colored relatively well-sorted plane parallel-stratified sediments of FA 4a suggests (1) higher energy and more stable current conditions within the system compared to FA 3, (2) a more oxygenated water column, oxidizing the iron present in the sediments, (3) a potential change in sediment sourcing, now originating from more homogeneous very fine to fine-grained sand-rich continental strata with a potential higher K-feldspar content, and (4) a short-lived relative sea-level drop with subaerial exposure. The channels of FA 4b are regarded as distal subtidal channels, due to the lack of intertidal indicators and the absence of any evidence of subaerial exposure, as well as the interfingering with the subtidal deposits of FA 3a and FA 3b. They are also regarded as the distal time correlative unit of the more proximal FA 4a. Also, the two incision events of FA 4b documented at Sven's Gulch (figure 4) might relate to the short lived relative sea-level fall and subsequent subaerial exposure episodes of FA 4a. The fact that the first incision carves deeper into the deposits of FA 3 implies a more important relative sea-level fall during the first episode of incision than during the second incision. FA 4 architecture and paleocurrent directions suggest a dominant basinward ebb-flow direction and a subordinate flood-tide in the lower part of the Curtis Formation.

Interestingly, the basal conglomerate documented at Last Chance Desert (figure 1, Facies F) is interpreted as flash-flood deposits resting directly on Pipiringos and O'Sullivan's (1978) J-3 unconformity, which implies that these deposits are older than the Curtis Formation as defined by Gilluly and Reeside (1928), yet younger than the Entrada Sandstone.

FA 5 – Sub- to Intertidal Channel-Dune-Flat Complex

Description

FA 5 is present in every locality in this study, with the notable exception of Little Flat Top (figures 1 and 3). In comparison with the underlying FA 3 and 4 deposits, the sand-dominated interval corresponding to FA 5 is relatively homogeneous (figure 8). FA 5 is easily identifiable in the field by its light green-white color, as well as its polished weathering appearance. It generally overlies FA 3 or FA 4, but between the measured sections Interstate 70 and Uneva Mine Canyon (figure 1), FA 5 caps FA 2 and FA 1 at a noticeable angle (figures 8F and 8G). FA 5 rests directly on FA 1 in sectors 2 and 3, with the exception of the Hanksville section, and is absent from Little Flat Top (figures 1, 2, and 3). The thickness and, to a lesser extent, the stacking architecture of this sedimentary unit strongly vary between studied sections, nevertheless displaying a southward-thinning trend, reaching more than 45 m thick at Stove Gulch, about 15 m thick at Interstate 70, and only 4.60 m thick at Hanksville (figures 1, 2, and 3). It also thins towards the east, measuring only about 1.30 m thick at Duma Point and about 0.8 cm thick at Crystal Geyser, but never exceeding 3.80 m thick in sector 3 (figures 1 and 3). Its lower sharp contact is either conformable with the underlying strata, onlapping its substratum, or erosive in nature, and corresponds to the MTS. FA 5 is dominated by sand-rich facies, featuring sedimentary structures such as flaser bedding (Facies N), climbing ripples (Facies O), or thoroughly rippled intervals, dominated by herringbone cross-stratification (Facies R). Some bedding surfaces display interference ripple marks that are arranged in a nearly orthogonal pattern. Fine-grained

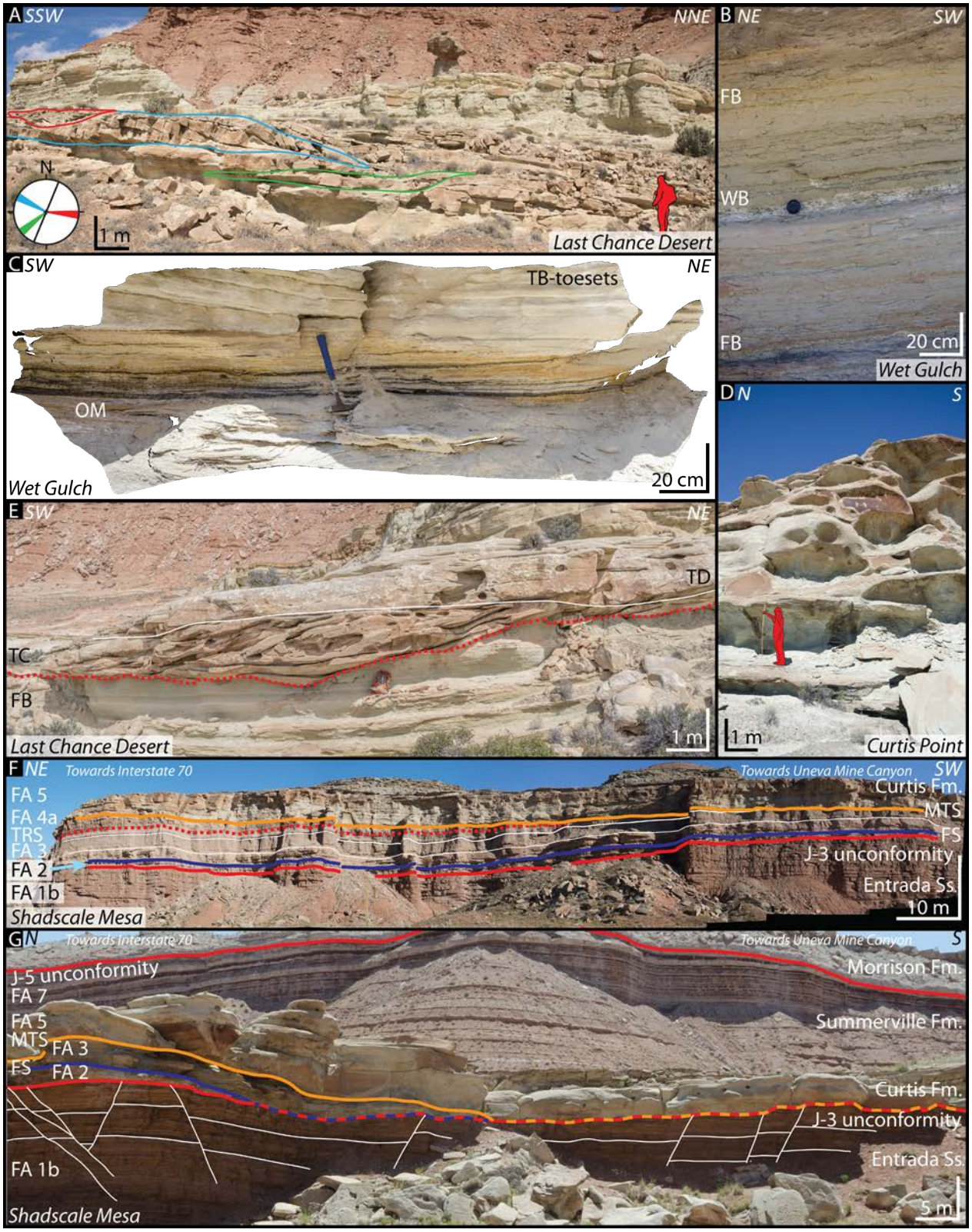

Abbreviations:
FB - Flaser Bedding OM - Organic Matter TB - Tidal Bundle TC - Tidal Channel TD - Tidal Dune WB - Wavy Bedding

Figure 8. Caption on the following page.

Figure 8 (figure on the previous page). Overview of FA 5 (middle Curtis). (A) Bidirectional tidal inlets (red and blue contours), and a third south-westward laterally accreting tidal channel (green contour) within a sub- to intertidal flat surrounding environment. The respective migration direction of these three bedforms is color-coded on the rose-diagram, whereas the black line on the diagram illustrates the outcrop orientation. (B) Heterolithic sandstone with an alternation of flaser bedding (FB, Facies N) and wavy bedding (WB, Facies M). Lenses cap: 67 mm. (C) Enrichment of organic matter (OM) in the toesets of certain rhythmic tidal bundles (Facies P). (D) Weathered surface of a structureless sandstone. (E) South-westward laterally accreting tidal channel, incising into subtidal sandstone with flaser bedding (FB). The channel was subsequently overlain by 3D tidally influenced dunes (TD) migrating towards the northeast. (F and G) The two pictures are respectively taken 1.3 and 2.2 km south of the Interstate 70 measured section. They show the erosive and angular relationship between FA 5 and its substratum, as the Curtis Sea was transgressing its poorly consolidated and uplifted substratum. The MTS at the base of FA 5 can be traced over the entire study area.

material arranged in laminated mudstone to lenticular to wavy bedding is recorded at Smith's Cabin (Facies K, L, M, figure 1). Other sedimentary structures and type of architecture can be observed, such as (1) locally amalgamated cm- to m-scale tidal bundles with varying amount of organic matter captured within their toesets (Facies P), (2) 3D dunes cut by several reactivation surfaces on top of which counter ripples can sometimes be seen (Facies C), and (3) plane parallel-stratified intervals (Facies S). These facies interfinger with one another over about 5 to 40 m. Both single and double mud drapes as well as desiccation cracks occur within several horizons included in FA 5.

The fact that three shallow core-drilling attempts through these sandstone beds failed at providing any usable cored plugs suggests the unit is poorly consolidated, at least through its first 20 cm, but the degree of consolidation varies significantly over tens of meters. Weathering can obscure sedimentary structures, which results in a structureless appearance (Facies Q). The stacking pattern of these different facies is extremely intricate, and each locality has subtly unique architecture. Therefore, the internal complexities of FA 5, coupled with distance between each location, render the detailed correlation between the measured sections very challenging and incompletely constrained. Note that the thickness, size, and wavelength of tidal structures diminish up-section, whereas the lower half of FA 5 displays a relatively constant scale of sedimentary architecture. Towards the east, in sector 3, FA 5 is dominated by rippled cross-laminated to undulated beds, with scattered structureless intervals. Current data are shifted in comparison with the underlying units, from a north-dominated to a more symmetrical northwest to southeast trend (figure 3). However, FA 5 shows similarities with the underlying facies associations, as recordings of a west-southwest to southwest flow direction are rare.

Interpretation

The overall high sand-to-mud ratio within FA 5 indicates an elevated energy level within the depositional environment, in comparison with the underlying units. However, this energy level fluctuated through space and time, as testified by the nature and the varying scale of the documented sedimentary structures, as well as by the intricate lateral and vertical interfingering and stacking pattern of the different facies. All of these features display the effect of individual and multiple tide cycles over a tidal flat (Facies C, L, M, N, O, and R), as well as neap-spring tidal cyclicity within a tidal channel (Facies P) (Kreisa and Moiola, 1986; Middleton, 1991; Nio and Yang, 1991; Fan, 2012; Hughes, 2012; Daidu, 2013). Ephemeral episodes of subaerial exposure occurred, as evident by desiccation cracks and, to a lesser extent, single intertidal mud drapes, typical for intertidal zones. Tidal channels are present, but never quite reach the size of the tidal channels observed in the underlying FA 3 as their lateral extent remains on the order of the decameter (dkm) with well-developed laterally accreting architecture (Facies I, figure 8E). The occurrence of other tidal channels is indicated by the presence of herringbone cross-stratification and sigmoidal tidal bundles (Kreisa and Moiola, 1986; Hughes, 2012). Considering this coastal setting, a highly various and undulating coastline is suggested, which Caputo and

Pryor (1991) and Wilcox and Currie (2008) bring forth and visualize by their paleoenvironment reconstruction models. As depositional energy conditions increase basinward, the clear change in grain size in comparison with the underlying finer grained deposits of FA 2, FA 3, and FA 4 and the extended erosive tidal ravinement surface at the base of FA 5 suggest an overall transgression within a context of limited available accommodation space, with the emplacement of high energy tidal channels and bars system, shielding the back barrier intertidal mix-flat in the southeast (FA 6) (see Dalrymple and others, 2012). The overall FA 5 interval corresponds to Flemming's (2012) bare tidal flat depositional system. The diminishing thickness, size, and wavelength of tidal structures up-section, as well as towards the east and the south, is interpreted to represent a decrease of tidal amplitude and influence over the study area as a result of the early stage of a prograding coastline within an asymmetrical, eastward-pinching foreland basin, which followed a period of architectural aggradation.

FA 6 – Upper Heterolithic Sub- to Intertidal Flat

Description

FA 6 (figure 9) represents the topmost overall finning-upward heterolithic interval of the Curtis Formation documented throughout the whole study area, but its occurrence is limited in sector 3 in comparison with the neighboring sectors 1 and 2. It conformably overlies the sand-dominated FA 5, whereas, at Little Flat Top, it directly overlies FA 3. Its thickness is fairly constant, gently varying between about 7 and 17 m. Internal structures include asymmetrical current- and wave-ripple lamination of Facies L, M, and N, interbedded with laminated mudstone, and structureless or planar parallel-stratified sandstone (Facies C, K, S). FA 6 is also marked by an increase of unidirectional current ripple lamination (Facies U), whereas bidirectional herringbone cross-laminations become increasingly sparse. Individual beds are as much as 10 to 40 cm thick. Dark-red paleosol horizons and scattered desiccation cracks, as well as scattered evaporite-rich levels are recorded throughout the successions. Reddish to orange-colored chert nodules often arranged along well-defined horizons are also common within FA 6. Paleocurrent data must be regarded with caution due to the low number of measurements (figure 3). Further, FA 6 sees the return of bioturbation, exclusively consisting of root burrows. FA 6 is characterized by an extreme scarcity, and a dramatically reduced bioturbation size, which would correspond to Droser and Bottjer (1986) ichnofabric index n°2. Note that once again the Crystal Geyser section remains an outcast, as the 2 to 5 m of interpreted Curtis Formation displays only Facies S, U, and X.

Interpretation

The alternation of heterolithic deposits such as in FA 6 is closely related to systematic and periodic energy level fluctuations, typical of a tide-influenced environment (Kvale, 2012). In comparison with the underlying units, the amplitude of flow velocity change, as well as the available accommodation is reduced, as suggested by the limited thickness of each bed and the size of the bedforms populating them. The disappearance of relatively deep tidal channel-related herringbone cross-lamination and its gradual replacement by an increased frequency of unidirectional landward-oriented washover deposits directly reflects a reduced rate of relative sea level rise, which marks the onset of a normal regression (Highstand System Tract [HSST]). The development of FA 6 is accompanied by a weaker tidal and overall marine influence over the intertidal flat, which generates extremely stressed habitability conditions within the system (Jaglarz and Uchman, 2010) coupled with episodes of subaerial exposure, as supported by precipitation of gypsum, the desiccation cracks, and the development of superficially vegetated paleosol horizons. FA 6 represents a more restricted and more proximal depositional environment than its FA 5 basinward equivalent.

FA 7 – Coastal Dry Eolian Dune Field

Description

FA 7 corresponds to the eolian deposits of the Moab Member of the Curtis Formation, which crop out in the vicinity of Moab and Arches National Park, Utah (figure 1). The overall thickness of FA 7 is as much as 50 m

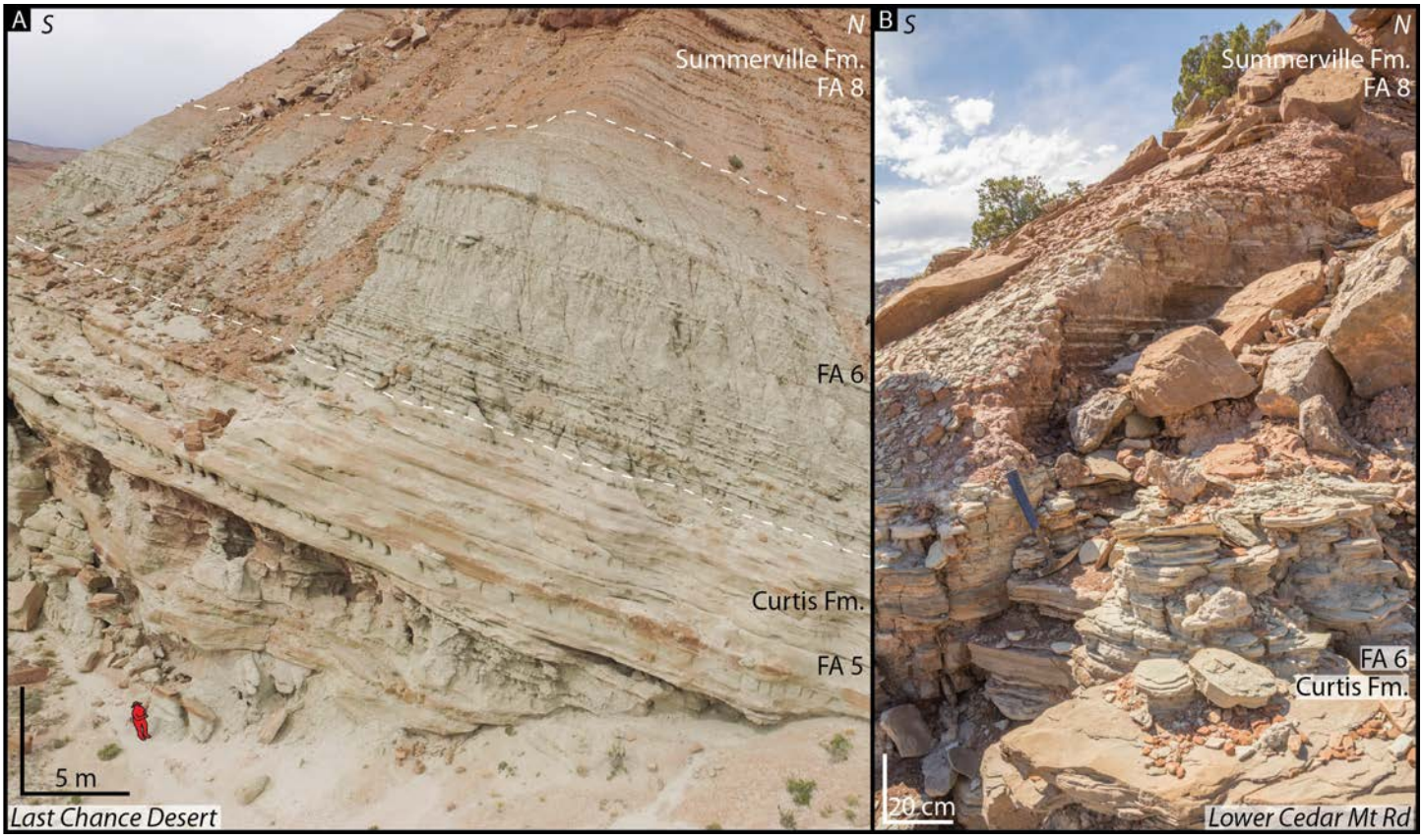

Figure 9. (A) Photo illustrating the conformable contact between the middle Curtis (FA 5), the upper Curtis (FA 6), and the Summerville Formation (FA 8), accompanied their upward-thinning and upward-finning of the beds. (B) Close up of the conformable contact between the upper Curtis and the Summerville Formation. The lithostratigraphic boundary lies at the top the hammer handle.

in the easternmost visited localities and pinches out a few 100 m east of Duma Point (figures 1 and 3). It rests directly on the Slick Rock Member of the Entrada Sandstone in the east and on the earthy facies towards Duma Point (figure 1). It is characterized at its base by a sedimentary package that mainly consists of light-green to white, structureless to ripple to trough cross-stratified, very fine to fine-grained sandstone (Facies Q and U), with greenish-colored silty sandstone intervals (Facies L), and superficial paleosols (Facies X). Facies Q and U are over-represented with respect to Facies X in the west, whereas this ratio inverts itself towards the east. Note that this facies has not been observed at Dewey Bridge section (figure 10). Soft-sediment deformation is common. This basal unit is overlain by a 1- to 3-m-thick, planar parallel-stratified, white fine-grained sandstone (Facies S), with locally occurring 0.3- to 0.5-m-thick tangential cross-stratified sandstone (Facies A) sets. The rest of the succession consists of four to five packages of amalgamated, large-scale (>2 m) tangential cross-stratified, fine-grained white sandstone (Facies A). The maximum height of individual foreset reaches about 15 m. Each of these sedimentary packages is truncated at their top by a supersurface, upon which paleosols (Facies X) and/or fine-grained, undulating to rippled cross-stratified white sandstone (Facies U) that is as much as 1 m thick can be observed. Note that rhizoliths can be visible up to 2 m below these supersurfaces (figures 10C and 10D). FA 7 can be capped by a thin 10- to 20-cm-thick, fine-grained, structureless yellow sandstone (Facies T).

Interpretation

The thick, tangential cross-stratified sandstone beds are interpreted as migrating compound eolian dunes (Facies A), with alternating grain-fall and grain-

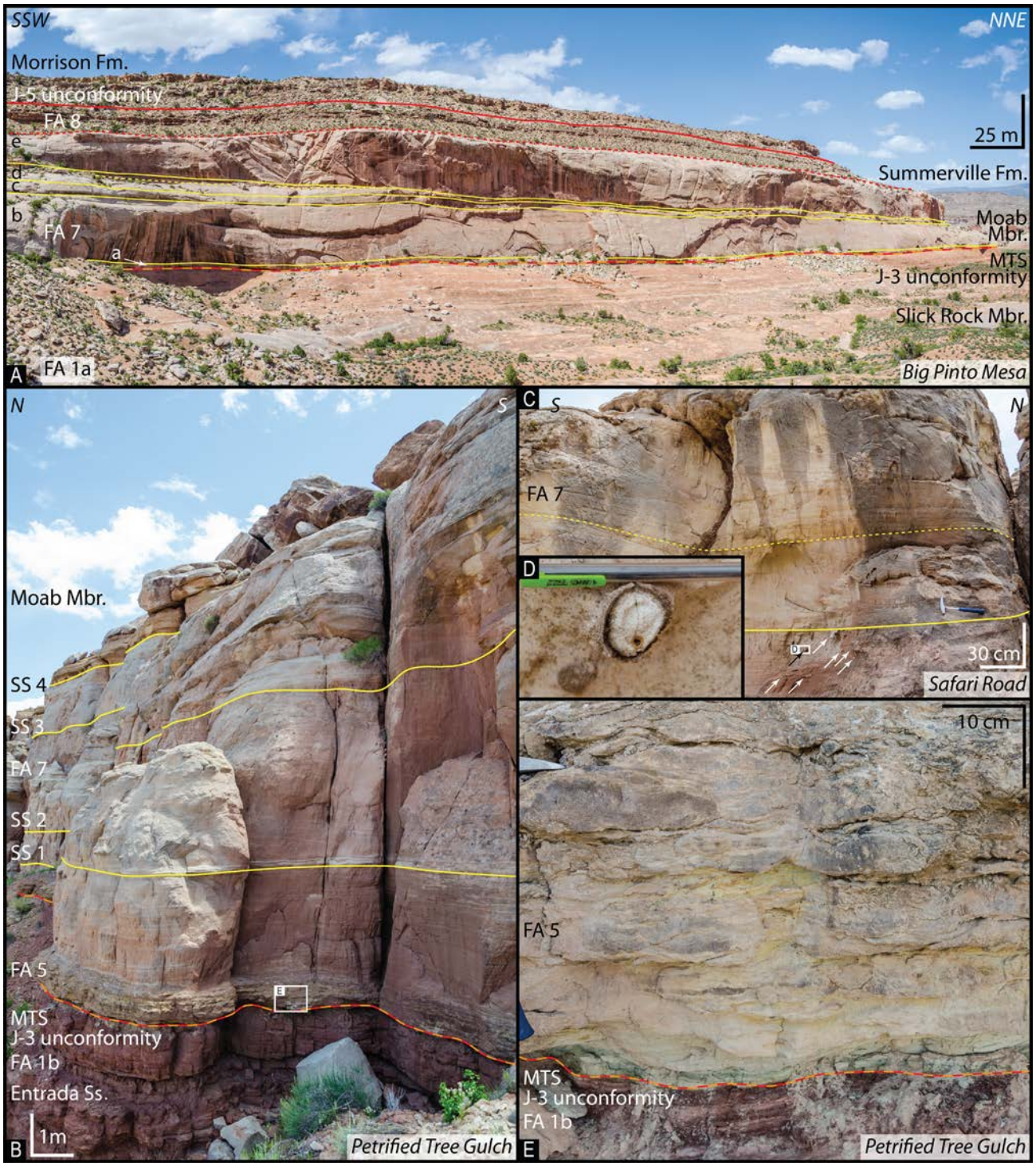

Figure 10. (A) Picture of the Moab Member (MTMb; FA 5 and FA 7) at Big Pinto Mesa, where a 50-m-thick section was measured through the eolian deposits of FA 7. It can be divided in five sequences (a-e). The MTMb crops out in sector 3 (see figure 3), and it overlies the earthy facies (FA 1b) in the western part of sector 3, whereas it rests directly on the Slick Rock Member (FA 1a) towards the east. (B, C, D, and E) Close-up photographs of the lowermost meters of FA 7, which conformably overlies water-carried sediments of FA 5. Each eolian sequence is capped by a supersurface (SS). Rhizoliths and their precipitation fronts (white arrows, and close-up D) can be present up to several decimeters below such a supersurface. They indicate that vegetation developed prior to the deposition of the following sequence.

flow deposits on the foresets of each dune. The westward-pinching geometry of FA 7 indicates that the main eolian depocenter was, at the time, located in the vicinity of Big Pinto Mesa (figure 1). The extent of the Moab Member (FA 7) suggests that the paleo-erg covered an area of at least 1800 km^2. However, this surface is certainly underestimated, due to the low preservation potential of eolian deposits (Rodríguez-López and others, 2014), as well as the limited area where the Moab Member has not yet been eroded.

The vertical stacking architecture of FA 7 makes it no stranger to the Kocurek (1988, 1999), Kocurek and Lancaster (1999), and Mountney (2006) cyclic depositional pattern: (1) construction, (2) accumulation, and (3) preservation phases of eolian deposits. The occurrence of the basal Facies Q, U, and L implies a marine incursion within a coastal plain domain, during a period of optimal climatic conditions allowing the development of (superficial) paleosols. Note that, when traced basinward, this basal tidally influenced marginal marine interval corresponds to the transgressive deposits of FA 5, which highlights the spatial extent of this major transgressive event, whereas the intervals characterized by Facies U represent short-lived marine transgression as FA 6 was being deposited farther to the west. The transition from a "wet" environment to a dry phase of eolian accumulation is accompanied by the deposition of sand sheets (Facies S) and small-scale eolian dunes (Facies A). The onset of this shift results from an increased amount of loose sediment available for wind transport, as a consequence of a lowering of the saturated level within the sedimentary column (Kocurek, 1988, 1999; Kocurek and Lancaster, 1999; Mountney, 2012). The replacement of small-scale bedforms by large-scale eolian dunes represents the major phase of accumulation, also indicative of peak aridity and highest loose sediment budget. Each eolian dune package (Facies A) is capped by laterally extensive deflation surfaces, which are referred to as supersurfaces (Brookfield, 1977; Talbot, 1985; Kocurek, 1988; Havholm and Kocurek, 1994), resulting from the cannibalization of the system down to the water saturated level, as the sand supply became exhausted. Similar to Mountney's (2006) models from the Permian Cedar Mesa Sandstone, the observed supersurfaces are also characterized, at least locally, by "abundant calcified rhizoliths and bioturbation and which represents the end product of a widespread deflation episode" (Mountney, 2006), and the potential development of superficial vegetation. The stacking of four to five of these eolian sequences suggests cyclic climatic alternations between humid and arid episodes (Mountney 2006, 2012). The near absence of interdune deposits, and the wedge-symmetry of the succession, assign FA 7 to a dry temporally and spatially dynamic eolian system (Kocurek and Havholm, 1993; Mountney, 2012).

FA 8 – Supratidal Flat

Description

FA 8 marks the stratigraphic top of this study and corresponds to the lowermost strata of the Summerville Formation, which is observed at each measured section (figure 9). FA 8 is characterized by a gradual yet short-lived transition from mostly greenish-colored tide-influenced strata (FA 6) into a succession dominated by dark-red laminated mudstone (Facies V), paleosols (Facies X), and evaporite-rich horizons. In the eastern part of the study area, FA 8 overlies FA 7, and the transition between the two units is abrupt, with no evidence of erosion. Centimeter- to decimeter-scale (cm- to dm-scale), light- to dark-green-colored, ripple-laminated strata (Facies U) and multi-dm-thick, trough cross-stratified sandstone beds (Facies I) occur repeatedly in FA 8. Facies U occurs ubiquitously within FA 8, whereas Facies I has been documented only in the eastern part of the study area. Both their number and thickness diminish up-section. Episodic but rare interbedded, fluvial-dominated strata (Facies W) occur within the succession. Note that both Facies U and Facies W locally display desiccation cracks.

Interpretation

Fine-dominated grain size, fairly well-sorted, small sedimentary structures, architecture, dark-red colors and evaporites suggest a quiet and arid coastal environment, with episodic seasonal fluvial floods as well as periodic short-lived marine incursions, marked by the thin greenish-colored ripple-laminated and thicker

trough cross-stratified beds. The fact that marine floods diminish up-section indicates a basinward-prograding coastline during a phase of normal regression (HSST).

DISCUSSION

Sector 1, Sector 2, and Sector 3

The study of these facies associations shows that the Curtis Formation, as defined by Gilluly and Reeside (1928) at their type section at Curtis Point (figure 1), can be divided in three lithostratigraphic sub-units easily identifiable in the field. These units are herein referred to as the lower, middle, and upper Curtis (informal nomenclature). The lateral equivalent Moab Member was originally defined by Wright and others (1962) as a member or a tongue of the Entrada Sandstone at the time. Doelling (2001) officially reassigned these eolian deposits as a member of the Curtis Formation. The spatial distribution of these three sub-units shows that the Curtis Formation displays three different expressions of itself over the study area, which are herein delimitated as sectors 1, 2, and 3.

The complete sub-unit trilogy of the Curtis Formation are only found in sector 1 (figure 3), which extends north of Uneva Mine Canyon on the eastern limb of the San Rafael Swell monocline; however, the triptych character of the formation disappears south of Last Chance Desert on the western margin of the San Rafael Swell (figures 1 and 3). Sector 2 (figure 3) is dominated by the middle and upper Curtis, with the notable following exceptions: (1) Duma Point, where only the middle Curtis is exposed, (2) Little Flat Top, where the middle Curtis is absent, and (3) Hanksville, where the three sedimentary sub-units crops out again (figure 1). On figure 3B, Little Flat Top's pie chart displays a particular pattern in the sense that it reflects the uncertain location of the formation boundary between the Entrada Sandstone and the FA 4a of the Curtis Formation. At that specific locality, three lithological candidate boundaries remain, hence influencing the resulting ratio between the different facies associations present in the Curtis Formation. Sector 3 delineates the extent of the Moab Member of the Curtis Formation (figure 3).

Lower, Middle, and Upper Curtis

The lower Curtis crops out in sector 1, as well as at Little Flat Top and at Hanksville in sector 2 (figures 1, 2, and 3). Its base corresponds to the J-3 unconformity as defined by Pipiringos and O'Sullivan (1978). As shown in figures 4C and 4D, figures 5 and 6, as well as figures 8F and 8G, the unconformity is characterized by various types of relief formed by different processes, such as eolian deflation, and fluvial or tidal currents, which impacted the unconformity at various times. However, defining the base of the lower Curtis by this polygenetic and composite surface notably implies that the basal flash-flood conglomerates at Last Chance Desert (figure 1, Facies F) also belong to the Curtis Formation, despite predating and being genetically unrelated to the formation. Instead, if it is decided to define the base of the formation using the multi-faceted transgressive surface while regrouping genetically related shallow marine deposits only, then this basal conglomerate at Last Chance Desert would become a-formational, as it would neither belong to the Entrada Sandstone nor the Curtis Formation. For lithostratigraphic convenience, it is suggested to use the highly diachronous J-3 unconformity of Pipiringos and O'Sullivan (1978) as the boundary for the lower Curtis, and thus keep these basal conglomerate within this sub-unit.

The lower Curtis is dominated by FA 3a-b dark-green to gray subtidal heterolithic strata, whereas FA 2 and FA 4 are present locally in the eastern part of sector 1, notably at Neversweat Wash, Sven's Gulch, Rabbit Gulch, and Interstate 70 (figures 1, 2, and 3). The ratio between the mud-dominated (FA 3a) and the sand-dominated heterolithic succession (FA 3b) varies spatially. The highest concentration of coarser-grained material, including conglomeratic beds, occurs in the western part of sector 1 at Lower Cedar Mountain Road and Last Chance Desert, whereas, on the eastern margin of sector 1, Sven's Gulch and Rabbit Gulch show similar enriched sand-to-mud ratios (figures 1, 2, and 3). The exact provenance of the different conglomeratic facies occurring in the Curtis Formation remains indeterminate. It is certain, however, that these extra-basinal lithoclasts are sourced from terrane(s?) exposed beyond the extent of the underlying strata of the Entrada Sand-

stone, due to the presence of metamorphosed polycrystalline quartz within these gravels and pebbles. Skeletal carbonate fragments of unidentified bryozoan also exclude the Entrada Sandstone as a potential source for these conglomeratic beds, as opposed to the bulk of the Curtis Formation, which has a modal composition similar to the underlying Entrada Sandstone (Dickinson and Gehrels, 2009, 2010). Despite the lack of provenance data, we suggest that these conglomerate beds represent reworked material, potentially from flash flood deposits, sourced from the uplifted highlands west of the study area (Thorman, 2011; Anderson, 2015) or from the nearby Uncompahgre highlands to the east of Moab (Otto and Picard, 1976; Scott and others, 2001). The fact that most dune-forming and channel-filling conglomeratic facies are in the lowermost meters of the lower Curtis suggests that, as the overall Curtis transgression proceeded, their sediment supply was exhausted. It seems that another sediment entry point emerged in the south to southeast parts of the study area, draining a different basin, from which reworked material from the Entrada Sandstone could have been assimilated into the Curtis Formation. Indeed, towards the south to southeast, FA 4a consists of relatively similar texture with respect to the underlying earthy facies of the Entrada Sandstone; it becomes increasingly dominant within the lower Curtis, as the heterogeneity and complex architecture of FA 3 is replaced by the laterally extensive, light-pink beds of FA 4a. The fact that no bleached front along fractures has been observed in this unit suggests that, unlike bleached fractures and corridors in the Carmel Formation and in the Entrada Sandstone (Ogata and others, 2014), no reducing fluids have circulated within these rocks (Skurtveit and others, 2017; Sundal and others, 2017; figures 4a and 7).

The middle Curtis consists exclusively of FA 5 deposits (figure 3), and its lower boundary corresponds to the MTS, which can sometimes display an erosional relief of about 50 to 90 cm and is hence locally identified as a tidal ravinement surface. In sector 1, the middle Curtis overlies the lower Curtis in a possibly conformable to disconformable to angular way, whereas in sector 2 and 3, the MTS merges with and partially reworks the J-3 unconformity (figure 8G). The angular unconformity between the lower and middle Curtis, visible south of Interstate 70 (figures 8F and 8G), suggests a sub-regional pre-middle Curtis uplift in the area which may signal regional yet unidentified tectonic activity over the area during the Late Jurassic, prior to the deposition of the middle Curtis. Further, local to sub-regional dome features, ascribed to sandy substratum mobility related to fluid overpressure and seismic activity (Jolly and Lonergan, 2002; Wheatley and others, 2016), are for instance visible 2.1 km north of Hanksville Airport, where the lower and middle Curtis display a fault system driven by an underlying, circular sand pillow (figure 4F). Just as for the J-3 unconformity, the terms unconformity and disconformity are to be taken with caution, as they imply, by definition, a significant time gap between the adjacent units (Van Wagoner and others, 1988; Holbrook and Bhattacharya, 2012), a temporal dimension, which, in the case of the Curtis Formation, cannot be assessed with great precision. The middle Curtis pinches out southward in sector 2 whereas it thins towards the east in sector 3. Due to the extreme low gradient present over the study area during the Jurassic (and through the Cretaceous) times (Heller and others, 1986; Fillmore, 1991; Lockley, 1991; Jones and Blakey, 1993), it is suggested that the time encapsulated in this transgression was short. This major and rapid transgression potentially reached far beyond the study area. Indeed, it may be linked to the deposition of the Todilto Formation and its calcareous saline sediments in southwestern Colorado and northwestern New Mexico (Lucas and Anderson, 1997), which were deposited after a blitz-flooding of the Entrada Sandstone by a marine incursion (Benan and others, 2000). It is important to note that other regional marine embayments co-existed with the Curtis sea in similar low-gradient conditions, such as the Ralston Creek Lobe of Anderson and Lucas (1994) in southeastern Colorado. Thus, the Todilto Formation is likely related to the MTS and to the base of the middle Curtis, which implies that the paleo-erg of the Entrada Sandstone existed in New Mexico until "instantaneous" transgression of Benan and others (2000), whereas it was cannibalized by the lower Curtis transgression in Utah.

The upper Curtis mainly consists of FA 6 deposits, with mud- and sand-dominated channel and tital-flat complexes. It has been recorded at each visited locality

in sectors 1 and 2, with the notable exception of Duma Point (figure 3). Its lower boundary is gradational, as it conformably overlies the middle Curtis. The main differences between the middle and upper Curtis reside in the up-section's increased heterogeneity, as well as a more pronounced green color, and the gradual replacement of the multi-m-thick bedforms by smaller scale sedimentary structures and thinner strata. It implies that the rate of accommodation decreased in the basin, whereas the sediment supply remained either constant, or potentially increased. The upper Curtis corresponds to the laterally equivalent Moab Member, which crops out in sector 3. The Moab Member is characterized by the dominance of the eolian dunes of FA 7 arranged in four to five distinct sequences, representing at least 78% of the Curtis Formation in the eastern part of the study area. The remaining percentages are recorded as a thin basal middle Curtis interval, whereas marine incursions (FA 6) or superficial paleosols and supratidal deposits (FA 7) separate the different eolian sequences (figure 10). Note that the base of the Summerville Formation (FA 7), which stratigraphically overlies the Curtis Formation conformably in the study area despite their obvious lateral stratigraphic relationship on a more regional scale, suffers from the same gradual transition, from which no evident lithological boundary rises. It is therefore proposed to define the base of the Summerville Formation as the line where, over a meter of succession, more than 50% of the deposits belong to the supratidal FA 8.

SPATIAL DISTRIBUTION OF THE VARIOUS FACIES ASSOCIATIONS: ILLUSTRATION BY MODERN ANALOGS

No modern analogs exist to fully illustrate the overall Curtis Formation depositional evolution. Nevertheless, as shown in figure 11, the inner Gulf of California and the Wadden Sea are suggested to represent similarities to the aforementioned Curtis Formation subdivisions. Such comparisons have limitations, and mainly regard spatial extent of modern environments in comparison with the size of their respective Curtis Formation counterparts, as well as basinal geometry approximations. The modern analogs are not meant to represent a similar tectonic setting to the Curtis Formation foreland basin conditions.

The lower Curtis is compared the fluvially starved, arid and unprotected tide-dominated bay of Las Lisas, Mexico (figure 11) (UTM coordinates: 12R 221191/3504767), on the northeastern margin of the Gulf of California. The bay offers a window on a probable convoluted facies belt arrangement which occurred during one of the lower Curtis short-lived regressive episodes. In the case of Las Lisas, such a regression is linked to rift flank uplift in the Neogene (Mark and others, 2014). As displayed on figure 11, the area close to the shoreline features sand-rich deposits similar to FA 4a interfingering with finer-grained, supratidal sediments of FA 8 and possibly conformably overlying pre-existing substratum (equivalent of FA 1a). Farther into the basin, the heterolithic subtidal flat deposits of FA 3 are interfingering with gravel-bearing tidal channels (FA 4b) and migrating dunes (Facies H).

The middle Curtis is paralleled with the Dutch part of the shielded and tide-dominated shallow Wadden Sea (figure 11; UTM coordinates: 31U 650032/5902807), where intricate and dynamic interplay of sub- to intertidal channels, tidal flats, and migrating tidal dunes and shoals (FA 5) has developed over an extensive and gently sloping area, behind barrier islands, as a result of a major and quick transgression (linked to Holocene glacio-eustatic sea-level rise in the Wadden Sea (Oost and de Boer, 1994)). It is important to point out that similar well-defined barrier islands are not recognized in the middle Curtis deposits (FA 5), although evidences for subaerial exposure episodes have been documented.

The selected paragon for the upper Curtis is the fluvially starved and arid, back-barrier bay of La Pinta, located 75 km to the southeast of Las Lisas (figure 11) (UTM coordinates: 12R 286227/3460602). Here, the sub- to intertidal sediments (FA 6) deposited in this protected environment are being progressively overlain by supratidal deposits (FA 8), as the underfilled depocenter morphs into an overfilled basin. It is accompanied by a seaward migration of the coastline, leading to the potential development of an eolian dune system (FA 7) in the neighboring area as sediments become subsequently available for transport (Carr-Crabaugh and Kocurek, 1998; Mountney, 2012).

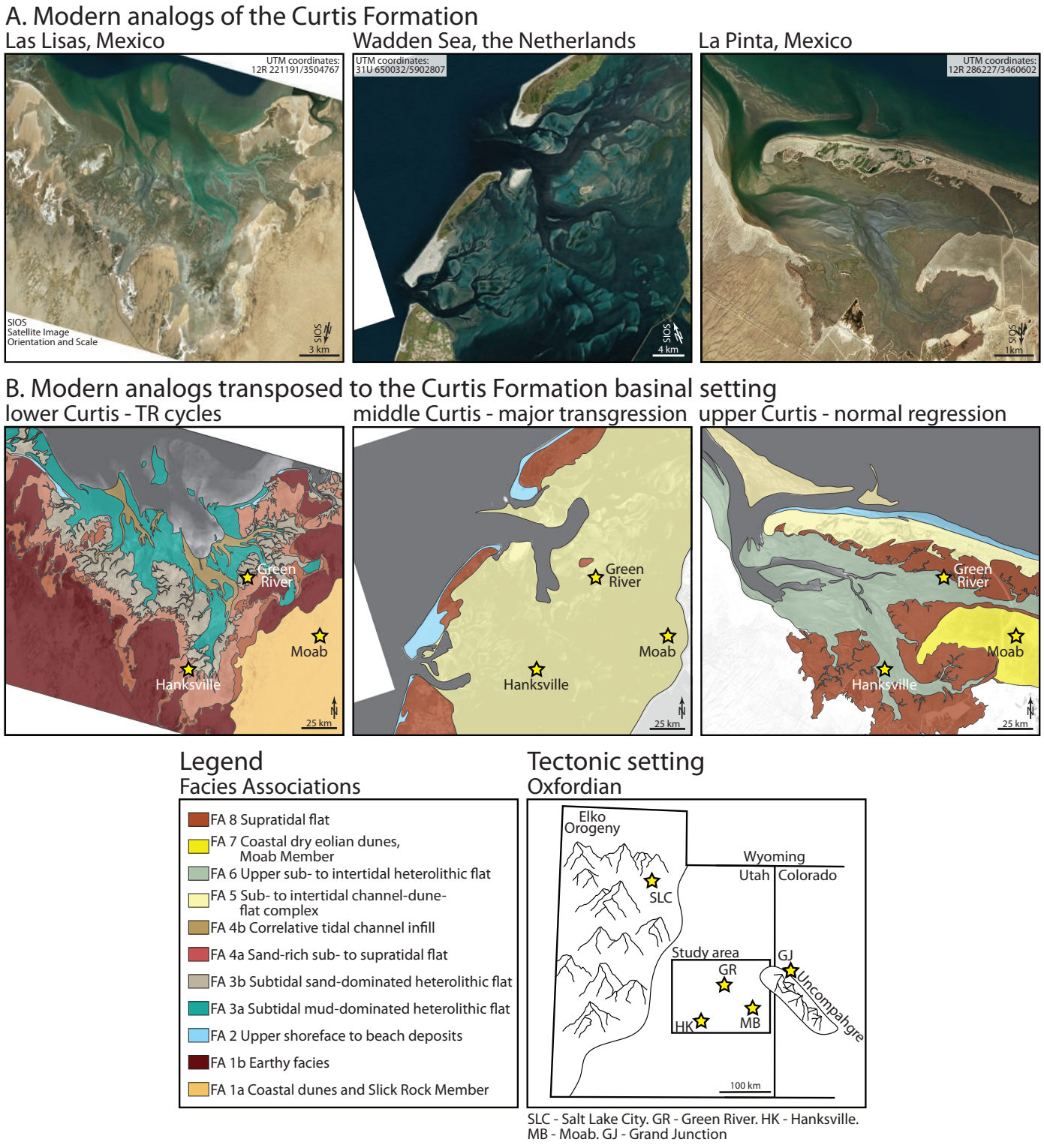

Figure 11. (A) Modern analogs of the lower, middle, and upper Curtis Formation, respectively. Note that these pictures are not aligned to the true north, but are rotated in a way that allows them to fit the orientation of the Curtis basin (satellite images from Microsoft Bing Maps). (B) Modern analogs draped with the corresponding facies associations from the Curtis Formation. The change of scale between A and B illustrates how much bigger the Curtis basin setting is with respect to the three modern analogs. TR cycles – transgressive-regressive cycles. Tectonic setting after Heyman (1983) and Thorman (2011).

CONCLUSIONS

1. Eight main facies associations (FA), including six sub-facies associations, were identified based on lithology, internal sedimentary structures, architectural arrangements, and spatial relationships. These facies associations are regarded as diagnostic expressions resulting from tidal processes in a fluvially starved, low-gradient, semi-enclosed epicontinental basin.
2. It is proposed to divide the Curtis Formation into three sub-units: the lower, middle, and upper Curtis. The specific spatial distribution of these sub-units allows the distinction of three different sectors across the study area: sector 1 in the north, sector 2 in the south-southwest, and sector 3 in the east.
3. The lower Curtis consists of laterally restricted upper shoreface to beach deposits (FA 2) overlain by a subtidal mud-dominated heterolithic succession (FA 3a), which grades into a sand-dominated subtidal flat (FA 3b). FA 3a and FA 3b interfinger with the more proximal and shallower FA 4a sand-rich sub- to supratidal flat, as well as with its more distal FA 4b correlative tidal channel infill.
4. FA 5, which corresponds to the middle Curtis, is mainly composed of a characteristic light green to white, very fine to fine-grained sandstone, appearing as an intricate arrangement of tidal channels, dunes, and tidal flats. The base of the middle Curtis coincides with the MTS, which can be traced throughout the entire study area.
5. The upper Curtis conformably overlies the middle Curtis and is characterized by heterolithic subtidal to intertidal deposits of FA 6, as well as their lateral and contemporaneous continental eolian dunes of the Moab Member (FA 7). The transition from the upper Curtis into the Summerville Formation is also gradual, with a progressively increasing occurrence of supra-tidal deposits (FA 8) within the succession.
6. The lower, middle, and upper Curtis occur in sector 1, whereas only the middle and the upper Curtis crop out in sector 2 (with local exceptions). Sector 3 corresponds to the area where the Moab Member of the Curtis Formation was deposited.
7. It is possible to compare the lower Curtis to the Bay of Las Lisas in the Gulf of California, the middle Curtis to the Wadden Sea in the Netherlands, and the upper Curtis to the bay of La Pinta in the Gulf of California.
8. The Todilto Formation or Todilto Member of the Wanakah Formation, which crops out in southwestern Colorado and northwestern New Mexico, is likely related to the major transgression that defines the base of the middle Curtis and is considered its lateral contemporaneous equivalent. Hence, the upper Wanakah Formation is regarded as the lateral equivalent of the Summerville Formation.
9. The middle Curtis overlies its substratum with an angular relationship on a sub-regional scale, suggesting an underlying and more regional deformational event during the Late Jurassic. Further, with the occurrence of local- to sub-regional collapse features within the lower and middle Curtis, the Late Jurassic must been impacted by episode(s) of sand mobility, which influenced the local surface morphology.
10. The J-3 unconformity exposed a composite nature, as it was impacted by various processes occurring before the Curtis Formation was deposited, as well as during the development of the lower and middle Curtis.

ACKNOWLEDGMENTS

The Norwegian Research Council is to be sincerely acknowledged, with their awarded grant COPASS 244049, which funded the first author and allowed the *ad hoc* conduct of the required field campaigns for this research. The authors would like to extend their gratitude to Dr. Anja Sundal, Anna van Yperen, Nathan "the Legend" Cote, Dr. Miquel Poyatos-Moré, Dr. Mark Mulrooney, Ole Rabbel, and Kristine Halvorsen for their assistance and helpful comments which elevated the standard of this work. Acknowledgments are to be extended to Grant C. Willis of the Utah Geological Survey (UGS) for his fruitful comments and review of an

early version of this manuscript. The authors also thank Kimm Harty (UGS) for her careful review and editing. Finally, we thank UGS technical editor Stephanie Carney, UGS Deputy Director Michael Hylland, and UGS Director Rick Allis for their reviews and support.

REFERENCES

Anderson, T.H., 2015, Jurassic (170–150 Ma) basins—the tracks of a continental-scale fault, the Mexico-Alaska megashear, from the Gulf of Mexico to Alaska, *in* Anderson, T.H., Didenko, A.N., Johnson, C.L., Khanchuk, A.I., and MacDonald, J.H., editors, Late Jurassic margin of Laurasia—a record of faulting accommodating plate rotation: Geological Society of America Special Papers 513, p. 107–188.

Anderson, O.J., and Lucas, S.G., 1994, Middle Jurassic stratigraphy, sedimentation and paleogeography in the southern Colorado Plateau and southern High Plains, *in* Caputo, M.V., Peterson, J.A., and Franczyk, K.J., editors, Mesozoic systems of the Rocky Mountain region, USA: Rocky Mountain Section SEPM (Society for Sedimentary Geology), p. 299–314.

Baas, J.H., 1999, An empirical model for the development and equilibrium morphology of current ripples in fine sand: Sedimentology, v. 46, no. 1, p. 123–138.

Barnard, P.L., Hanes, D.M., Rubin, D.M., and Kvitek, R.G., 2006, Giant sand waves at the mouth of San Francisco Bay: EOS Transactions American Geophysical Union, v. 87, no. 29, p. 285–289.

Benan, A., Cheikh, A., and Kocurek, G., 2000, Catastrophic flooding of an eolian dune field—Jurassic Entrada and Todilto Formations, Ghost Ranch, New Mexico, USA: Sedimentology, v. 47, no. 6, p. 1069–1080.

Bjerrum, C.J., and Dorsey, R.J., 1995, Tectonic controls on deposition of Middle Jurassic strata in a retroarc foreland basin, Utah-Idaho trough, Western Interior, United States: Tectonics, v. 14, no. 4, p. 962–978.

Blodgett, R.H., 1988, Calcareous paleosols in the Triassic Dolores Formation, *in* Reinhardt, J., and Sigleo, W.R., editors, Paleosols and weathering through time—principles and applications: Geological Society of America Special Papers 216, p. 103–121.

Bostock, J., and Riley, H.T., 1855, editors, Pliny the Elder, The Natural History: London Taylor and Francis, v. 2, book 16, chapter 1, unpaginated.

Boyd, R., Dalrymple, R., and Zaitlin, B.A., 1992, Classification of clastic coastal depositional environments: Sedimentary Geology, v. 80, no. 3-4, p. 139–150.

Brenner, R.L., and Peterson, J.A., 1994, Jurassic sedimentary history of the northern portion of the Western Interior Seaway, USA., *in* Caputo, M.V., Peterson, J.A. and Franczyk, K.J., editors, Mesozoic systems of the Rocky Mountain region, USA: Rocky Mountain Section SEPM (Society for Sedimentary Geology), p. 233–272.

Brookfield, M.E., 1977, The origin of bounding surfaces in ancient eolian sandstones: Sedimentology, v. 24, no. 3, p. 303–332.

Bump, A.P., and Davis, G.H., 2003, Late Cretaceous–early Tertiary Laramide deformation of the northern Colorado Plateau, Utah and Colorado: Journal of Structural Geology, v. 25, no. 3, p. 421–440.

Caputo, M.V., and Pryor, W.A., 1991, Middle Jurassic tide- and wave-influenced coastal facies and paleogeography, upper San Rafael Group, east-central Utah, *in* Chidsey, T.C., Jr., Geology of east-central Utah: Utah Geological Association Publication 19, p. 9–27.

Carr-Crabaugh, M., and Kocurek, G., 1998, Continental sequence stratigraphy of a wet eolian system—a key to relative sea-level change: Society for Sedimentary Geology Special Publication 59, p. 213–228.

Catuneanu, O., Abreu, V., Bhattacharya, J.P., Blum, M.D., Dalrymple, R.W., Eriksson, P.G., Fielding, C.R., Fisher, W.L., Galloway, W.E., Gibling, M.R., Giles, K.A., Holbrook, J.M., Jordan, R., Kendall, C.G.St.C., Macurda, B., Martinsen, O.J., Mial, A.D., Neal, J.E., Nummedal, D., Pomar, L., Posamentier, H.W., Pratt, B.R., Sarg, J.F., Shanley, K.W., Steel, R.J., Strasser, A., Tucker, M.E., and Winker, C., 2009, Towards the standardization of sequence stratigraphy: Earth-Science Reviews, v. 92, no. 1, p. 1–33.

Condon, S.M., and Huffman, A.C., Jr., 1988, Revisions in nomenclature of the middle Jurassic Wanakah Formation, northwestern New Mexico and northeastern Arizona: U.S. Geological Survey Bulletin 1633-A, p. A1–A12.

Crabaugh, M., and Kocurek, G., 1993, Entrada Sandstone—an example of a wet eolian system, *in* Pye, K., editor, The dynamics and environmental context of eolian sedimentary systems: London, Geological Society Special Publications No. 72, p. 103–126.

Daidu, F., 2013, Classifications, sedimentary features and facies associations of tidal flats: Journal of Palaeogeography, v. 2, no. 1, p. 66–80.

Dalrymple, R.W., Zaitlin, B.A., and Boyd, R., 1992, Estuarine facies models—conceptual basis and stratigraphic implications: Journal of Sedimentary Research, v. 62, no. 6, p. 1130–1146.

Dalrymple, R.W., Mackay, D.A., Ichaso, A.A., and Choi, K.S., 2012, Processes, morphodynamics, and facies of tide-dominated estuaries, *in* Davis, R.A., Jr., and Dalrymple, R.W., editors, Principles of tidal sedimentology: Dordrecht, Netherlands, Springer Science and Business Media, p. 79–107.

Davis, R.A., Jr., and Dalrymple, R.W., editors, 2012, Principles of tidal sedimentology: Dordrecht, Netherlands, Springer Sci-

ence and Business Media, 621 p.

De Gibert, J.M., and Ekdale, A.A., 1999, Trace fossil assemblages reflecting stressed environments in the Middle Jurassic Carmel seaway of central Utah: Journal of Paleontology, v. 73, no. 4, p. 711–720.

Dickinson, W.R., and Gehrels, G.E., 2009, U-Pb ages of detrital zircons in Jurassic eolian and associated sandstones of the Colorado Plateau—evidence for transcontinental dispersal and intraregional recycling of sediment: Geological Society of America Bulletin, v. 121, no. 3–4, p. 408–433.

Dickinson, W.R., and Gehrels, G.E., 2010, Insights into North American paleogeography and paleotectonics from U–Pb ages of detrital zircons in Mesozoic strata of the Colorado Plateau, USA: International Journal of Earth Sciences, v. 99, no. 6, p. 1247–1265.

Dickinson, W.R., Stair, K.N., Gehrels, G.E., Peters, L., Kowallis, B.J., Blakey, R.C., Amar, J.R., and Greenhalgh, B.W., 2010, U-Pb and $^{40}Ar/^{39}Ar$ ages for a tephra lens in the Middle Jurassic Page Sandstone—first direct isotopic dating of a Mesozoic eolianite on the Colorado Plateau: The Journal of Geology, v. 118, no. 3, p. 215–221.

Doelling, H.H., 2001, Geologic map of the Moab and eastern part of the San Rafael Desert 30' x 60' quadrangles, Grand and Emery Counties, Utah, and Mesa County, Colorado: Utah Geological Survey Map 180, 3 plates, scale 1:100,000.

Doelling, H.H., Kuehne, P.A., Willis, G.C., and Ehler, J.B., 2015, Geologic map of the San Rafael Desert 30' x 60' quadrangle, Emery and Grand Counties, Utah: Utah Geological Survey Map 267DM, 24 p., 2 plates, scale 1:62,500.

Doelling, H.H., Sprinkel, D.A., Kowallis, B.J., and Kuehne, P.A., 2013, Temple Cap and Carmel Formations in the Henry Mountains basin, Wayne and Garfield Counties, Utah, *in* Morris, T.H., and Ressetar, R., editors, The San Rafael Swell and Henry Mountains Basin—geologic centerpiece of Utah: Utah Geological Association Publication 42, p. 279–318.

Droser, M.L., and Bottjer, D.J., 1986, A semiquantitative field classification of ichnofabric—research method paper: Journal of Sedimentary Research, v. 56, no. 4, p. 558–559.

Eschner, T.B., and Kocurek, G., 1988, Origins of relief along contacts between eolian sandstones and overlying marine strata: American Association of Petroleum Geologists Bulletin, v. 72, no. 8, p. 932–943.

Fan, D., 2012, Open-coast tidal flats, *in* Davis, R.A., Jr., and Dalrymple, R.W., editors, Principles of tidal sedimentology: Dordrecht, Netherlands, Springer Science and Business Media, p. 187–229.

Fillmore, R.P., 1991, Tectonic influence on sedimentation in the southern Sevier foreland, Iron Springs Formation (Upper Cretaceous) southwestern, Utah: Geological Society of America Special Papers 260, p. 9–26.

Flemming, B.W., 2012, Siliciclastic back-barrier tidal flats, *in* Davis, R.A., Jr., and Dalrymple, R.W., editors, Principles of tidal sedimentology: Dordrecht, Netherlands, Springer Science and Business Media, p. 231–267.

Gilluly, J., and Reeside, J.B., Jr., 1928, Sedimentary rocks of the San Rafael Swell and some adjacent areas in eastern Utah: U.S. Geological Survey Professional Paper 150-D, p. 61–110.

Halland, E.K., Bjørnestad, A., Magnus, C., Riis, F., Meling, I.M., Tørneng Gjeldvik, I., Tappel, I.M., Mujezinović, J., Bjørheim M., Rød, R.S., and Pham, V.T.H., 2014, CO_2 storage atlas—Norwegian continental shelf: Stavanger, Norway, Norwegian Petroleum Directorate, not paginated.

Haq, B.U., Hardenbol, J., and Vail, P.R., 1987, Chronology of fluctuating sea levels since the Triassic: Science, v. 235, no. 4793, p. 1156–1167.

Hartwick, E., 2010. Eolian architecture of sandstone reservoirs in the Covenant field, Sevier County, Utah [abs.]: Geological Society of America, Abstracts with Programs, v. 42, p. 52.

Havholm, K.G., and Kocurek, G., 1994, Factors controlling eolian sequence stratigraphy—clues from super bounding surface features in the Middle Jurassic Page Sandstone: Sedimentology, v. 41, no. 5, p. 913–934.

Heller, P.L., Bowdler, S.S., Chambers, H.P., Coogan, J.C., Hagen, E.S., Shuster, M.W., and Lawton, T.F., 1986, Time of initial thrusting in the Sevier orogenic belt, Idaho-Wyoming and Utah: Geology, v. 14, no. 5, p. 388–391.

Heyman, O.G., 1983, Distribution and structural geometry of faults and folds along the northwestern Uncompahgre uplift, western Colorado and eastern Utah, *in* Averett, W., editor, Northern Paradox Basin-Uncompahgre uplift, Grand Junction Geological Society field trip, p. 45–57.

Hintze, L.F., 1980, Geologic map of Utah: Utah Geological and Mineral Survey, scale 1:250,000, 2 sheets.

Hintze, L.F., and Kowallis, B.J., 2009, Geologic history of Utah: Brigham Young University Geology Studies Special Publication 9, 225 p.

Holbrook, J.M., and Bhattacharya, J.P., 2012, Reappraisal of the sequence boundary in time and space—case and considerations for an SU (subaerial unconformity) that is not a sediment bypass surface, a time barrier, or an unconformity: Earth-Science Reviews, v. 113, no. 3, p. 271–302.

Hughes, Z.J., 2012, Tidal channels on tidal flats and marshes, *in* Davis, R.A., Jr., and Dalrymple, R.W., editors, Principles of tidal sedimentology: Dordrecht, Netherlands, Springer Science and Business Media, p. 269–300.

Imlay, R.W., 1947, Marine Jurassic of Black Hills area, South Dakota and Wyoming: American Association of Petroleum Geolo-

gists Bulletin, v. 31, no. 2, p. 227–273.

Imlay, R.W., 1980, Jurassic paleobiogeography of the conterminous United States in its continental setting: U.S. Geological Survey Professional Paper 1062, 134 p.

Jaglarz, P., and Uchman, A., 2010, A hypersaline ichnoassemblage from the Middle Triassic carbonate ramp of the Tatricum domain in the Tatra Mountains, southern Poland: Palaeogeography, Palaeoclimatology, Palaeoecology, v. 292, no. 1–2, p. 71–81.

Jolly, R.J., and Lonergan, L., 2002, Mechanisms and controls on the formation of sand intrusions: Journal of the Geological Society, v. 159, no. 5, p. 605–617.

Jones, L.S., and Blakey, R.C., 1993, Erosional remnants and adjacent unconformities along an eolian-marine boundary of the Page Sandstone and Carmel Formation, Middle Jurassic, south-central Utah: Journal of Sedimentary Research, v. 63, no. 5, p. 852–859.

Kampman, N., Maskell, A., Bickle, M., Evans, J., Schaller, M., Purser, G., Zhou, Z., Gattacceca, J., Petrie, E., and Rochelle, C., 2013, Scientific drilling and downhole fluid sampling of a natural CO_2 reservoir, Green River, Utah: Scientific Drilling, v. 16, p. 33–43.

Kocurek, G., 1988, First-order and super bounding surfaces in eolian sequences—bounding surfaces revisited: Sedimentary Geology, v. 56, no. 1–4, p. 193–206.

Kocurek, G., 1999, The eolian rock record (Yes, Virginia, it exists, but it really is rather special to create one), *in* Goudie, A.S., Livingstone, I., and Stokes, S., editors, Eolian environments, sediments and landforms: New York, Wiley, p. 239–259.

Kocurek, G., and Dott, R.H., Jr., 1983, Jurassic paleogeography and paleoclimate of the central and southern Rocky Mountains region, *in* Reynolds, M.W., and Dolly, E.D., editors, Mesozoic paleogeography of west-central United States–Rocky Mountain paleogeography symposium 2: Rocky Mountain Section SEPM (Society for Sedimentary Geology), p. 101–116.

Kocurek, G., and Havholm, K.G., 1993, Eolian sequence stratigraphy—a conceptual framework (chapter 16), *in* Weimer, P., and Posamentier, H., editors, Siliciclastic sequence stratigraphy—recent developments and applications: American Association of Petroleum Geologists Memoir 58, p. 393–409.

Kocurek, G., and Lancaster, N., 1999, Eolian system sediment state—theory and Mojave Desert Kelso dune field example: Sedimentology, v. 46, no. 3, p. 505–515.

Kowallis, B.J., Christiansen, E.H., Deino, A.L., Zhang, C., and Everett, B.H., 2001, The record of Middle Jurassic volcanism in the Carmel and Temple Cap Formations of southwestern Utah: Geological Society of America Bulletin, v. 113, no. 3, p. 373–387.

Kreisa, R.D., and Moiola, R.J., 1986, Sigmoidal tidal bundles and other tide-generated sedimentary structures of the Curtis Formation, Utah: Geological Society of America Bulletin, v. 97, no. 4, p. 381–387.

Kvale, E.P., 2012, Tidal constituents of modern and ancient tidal rhythmites—criteria for recognition and analyses, *in* Davis, R.A., Jr., and Dalrymple, R.W., editors, Principles of tidal sedimentology: Dordrecht, Netherlands, Springer Science and Business Media, p. 1–17.

Levander, A., Schmandt, B., Miller, M.S., Liu, K., Karlstrom, K.E., Crow, R.S., Lee, C-T.A., and Humphreys, 2011, Continuing Colorado Plateau uplift by delamination-style convective lithospheric downwelling: Nature, v. 472, no. 7344, p. 461–465.

Lockley, M.G., 1991, The Moab megatracksite—a preliminary description and discussion of millions of middle Jurassic tracks in eastern Utah, *in* Averett, W.R., editor, Guidebook for dinosaur quarries and tracksites tour—western Colorado and eastern Utah: Grand Junction Geological Society, p. 59–65.

Lucas, S.G., 2014, Lithostratigraphy of the Jurassic San Rafael Group from Bluff to the Abajo Mountains, southeastern Utah: Stratigraphic relationships of the Bluff Sandstone. Volumina Jurassica, v. 12, p. 55–68.

Lucas, S.G., and Anderson, O.J., 1997, The Jurassic San Rafael Group, Four Corners region, *in* Lucas, S.G., Anderson, O.J., and Kues, B.S., editors, Mesozoic geology and paleontology of the Four Corners region: New Mexico Geological Society, 48th Annual Fall Field Conference Guidebook, p. 115–132.

Mansfield, G.R., and Roundy, P.V., 1916, Revision of the Beckwith and Bear River Formations of southeastern Idaho: U.S. Geological Survey Professional Paper 98, p. 75–84.

Mark, C., Gupta, S., Carter, A., Mark, D.F., Gautheron, C., and Martín, A., 2014, Rift flank uplift at the Gulf of California—no requirement for asthenospheric upwelling: Geology, v. 42, no. 3, p. 259–262.

Martinius, A.W., Ringrose, P.S., Brostrøm, C., Elfenbein, C., Næss, A., and Ringås, J.E., 2005, Reservoir challenges of heterolithic tidal sandstone reservoirs in the Halten Terrace, mid-Norway: Petroleum Geoscience, v. 11, no. 1, p. 3–16.

McMullen, S.K., Holland, S.M., and O'Keefe, F.R., 2014, The occurrence of vertebrate and invertebrate fossils in a sequence stratigraphic context—the Jurassic Sundance Formation, Bighorn Basin, Wyoming, USA: Palaios, v. 29, no. 6, p. 277–294.

Middleton, G.V., 1991, A short historical review of clastic tidal sedimentology, *in* Smith, D.G., Reinson, G.E., Zaitlin, B.A., and Rahmani, R.A., editors, Clastic tidal sedimentology: Canadian Society of Petroleum Geologists Memoir 16, p. ix–xv.

Midtkandal, I., and Nystuen, J.P., 2009, Depositional architecture of a low-gradient ramp shelf in an epicontinental sea—the Lower Cretaceous of Svalbard: Basin Research, v. 21, no. 5, p. 655–675.

Mountney, N.P., 2006, Periodic accumulation and destruction of eolian erg sequences in the Permian Cedar Mesa Sandstone, White Canyon, southern Utah, USA: Sedimentology, v. 53, no. 4, p. 789–823.

Mountney, N.P., 2012, A stratigraphic model to account for complexity in eolian dune and interdune successions: Sedimentology, v. 59, no. 3, p. 964–989.

Murray, K.E., Reiners, P.W., and Thomson, S.N., 2016, Rapid Pliocene-Pleistocene erosion of the central Colorado Plateau documented by apatite thermochronology from the Henry Mountains: Geology, v. 44, no. 6, p. 483–486.

Nelson, S.T., 1997, Reevaluation of the central Colorado Plateau laccoliths in the light of new age determination: U.S. Geological Survey Bulletin 2158, p. 37–39.

Nio, S.D., and Yang, C.S., 1991, Diagnostic attributes of clastic tidal deposits—a review, *in* Smith, D.G., Reinson, G.E., Zaitlin, B.A., and Rahmani, R.A., editors, Clastic tidal sedimentology: Canadian Society of Petroleum Geologists Memoir 16, p. 3–28.

Nuccio, V.F., and Condon, S.M., 1996, Burial and thermal history of the Paradox Basin, Utah and Colorado, and petroleum potential of the Middle Pennsylvanian Paradox Formation: U.S. Geological Survey Bulletin 2000-O, p. 57–76.

Ogata, K., Senger, K., Braathen, A., and Tveranger, J., 2014, Fracture corridors as seal-bypass systems in siliciclastic reservoir-cap rock successions—field-based insights from the Jurassic Entrada Formation (SE Utah, USA): Journal of Structural Geology, v. 66, p. 162–187.

Ogg, J.G., Ogg, G., and Gradstein, F.M., 2016, A concise geologic time scale: Amsterdam, Netherlands, Elsevier, 240 p.

Oost, A.P., and de Boer, P., 1994, Sedimentology and development of barrier islands, ebb-tidal deltas, inlets and backbarrier areas of the Dutch Wadden Sea: Senckenbergiana Maritima, v. 24, no. 1, p. 65–115.

Otto, E.P., and Picard, M.D., 1976, Petrology of the Entrada Sandstone (Jurassic), northeastern Utah, *in* Hill, J.G., editor, Geology of the Cordilleran hingeline: Rocky Mountain Association of Petroleum Geologists Guidebook, p. 231–259.

Owen, G., Moretti, M., and Alfaro, P., 2011, Recognising triggers for soft-sediment deformation—current understanding and future directions: Sedimentary Geology, v. 235, no. 3–4, p. 133–140.

Parrish, J.T., and Peterson, F., 1988, Wind directions predicted from global circulation models and wind directions determined from eolian sandstones of the western United States—a compilation: Sedimentary Geology, v. 56, p. 261–282.

Peterson, F., 1988, Pennsylvanian to Jurassic eolian transportation systems in the western United States: Sedimentary Geology, v. 56, p. 207–260.

Peterson, F., 1994, Sand dunes, sabkhas, streams, and shallow seas—Jurassic paleogeography in the southern part of the Western Interior Basin, *in* Caputo, M.V., Peterson, J.A. and Franczyk, K.J., editors, Mesozoic systems of the Rocky Mountain region, USA: Rocky Mountain Section SEPM (Society for Sedimentary Geology), p. 233–272.

Peterson, F., and Pipiringos, G.N., 1979, Stratigraphic relations of the Navajo Sandstone to Middle Jurassic Formations, southern Utah and northern Arizona: U.S. Geological Survey Professional Paper 1035-B, 43 p.

Petrie, E.S., Sandul, A., Gutierrez, M., and Bratthen, A., 2017, Deformation band formation and reactivation associated with a Laramide fault propagation fold [abs.]: Geological Society of America Abstract with Programs, v. 49, no. 6, p. 289–299.

Pipiringos, G.N., and O'Sullivan, R.B., 1978, Principal unconformities in Triassic and Jurassic rocks, Western Interior United States—a preliminary survey: U.S. Geological Survey Professional Paper, 1035-A, 29, 1 plate, p. 1–29.

Pipiringos, G.N., and Imlay, R.W., 1979, Lithology and subdivisions of the Jurassic Stump Formation in southeastern Idaho and adjoining areas: U.S. Geological Survey Professional Paper 1035-C, 25 p.

Rodríguez-López, J.P., Clemmensen, L.B., Lancaster, N., Mountney, N.P., and Veiga, G.D., 2014, Archean to Recent aeolian sand systems and their sedimentary record—current understanding and future prospects: Sedimentology, v. 61, no. 6, p. 1487–1534.

Scott, R.B., Harding, A.E., Hood, W.C., Cole, R.D., Livaccari, R.F., Johnson, J.B., Shroba, R.R., and Dickerson, R.P., 2001, Geologic map of Colorado National Monument and adjacent areas, Mesa County, Colorado: U.S. Geological Map I-2740, 40 p., 1 plate, scale 1:24,000.

Sprinkel, D.A., Doelling, H.H., Kowallis, B.J., Waanders, G., and Kuehne, P.A., 2011, Early results of a study of Middle Jurassic strata in the Sevier fold and thrust belt, Utah, *in* Sprinkel, D.A., Yonkee, W.A., and Chidsey, T.C., Jr., editors, Sevier thrust belt—northern and central Utah and adjacent areas: Utah Geological Association Publication 40, p. 151–172.

Skurtveit, E., Braathen, A., Larsen, E.B., Sauvin, G., Sundal, A., and Zuchuat, V., 2017, Pressure induced deformation and flow using CO_2 field analogues, Utah: Energy Procedia, v. 14, p. 3257–3266.

Sullivan, K.R., Kowallis, B.J., and Mehnert, H.H., 1991, Isotopic ages of igneous intrusions in southeastern Utah—evidence for a mid-Cenozoic Reno–San Juan magmatic zone: Brigham Young University Geology Studies, v. 37, p. 139–144.

Sundal, A., Miri, R., Hellevang, H., Tveranger, J., Midtkandal, I., Zuchuat, V., Aagaard, P., and Braathen, A., 2017, Movement of CO_2 charged fluids in low permeability rocks during deformation—migration patterns in the Carmel Formation, Utah: En-

ergy Procedia, v. 114, p. 4537–4544.

Talbot, M.R., 1985, Major bounding surfaces in eolian sandstones—a climatic model: Sedimentology, v. 32, no. 2, p. 257–265.

Tape, C.H., Cowan, C.A., and Runkel, A.C., 2003, Tidal-bundle sequences in the Jordan Sandstone (Upper Cambrian), southeastern Minnesota, USA—evidence for tides along inboard shorelines of the Sauk epicontinental sea: Journal of Sedimentary Research, v. 73, no. 3, p. 354–366.

Thorman, C.H., 2011, The Elko orogeny—a major tectonic event in eastern Nevada–western Utah, *in* Sprinkel, D.A., Yonkee, W.A., and Chidsey, T.C., Jr., editors, Sevier thrust belt—northern and central Utah and adjacent areas: Utah Geological Association Publication 40, p. 117–129.

Trudgill, B.D., 2011, Evolution of salt structures in the northern Paradox Basin—controls on evaporite deposition, salt wall growth and supra-salt stratigraphic architecture: Basin Research, v. 23, no. 2, p. 208–238.

Turner, C.E., and Peterson, F., 1999, Biostratigraphy of dinosaurs in the Upper Jurassic Morrison Formation of the Western Interior, U.S.A., *in* Gillette, D.D., editor, Vertebrate paleontology in Utah: Utah Geological Survey Miscellaneous Publication 99-1, p. 77–114.

Urash, R.G., and Savrda, C.E., 2017, Ichnology of an Eocene shallow marine passive margin condensed section, eastern Gulf coastal plain, Alabama, USA: Palaeogeography, Palaeoclimatology, Palaeoecology, v. 471, p. 58–70.

Van Wagoner, J.C., Posamentier, H.W., Mitchum, R.M.J., Vail, P.R., Sarg, J.F., Loutit, T.S., and Hardenbol, J., 1988, An overview of the fundamentals of sequence stratigraphy and key definitions: Society of Economic Paleontologists and Mineralogists (SEPM) Special Publication No. 42, p. 39–45.

Waldschmidt, W.A., and LeRoy, L.W., 1944, Reconsideration of the Morrison Formation in the type area, Jefferson County, Colorado: Geological Society of America Bulletin, v. 55, no. 9, p. 1097–1114.

Wang, P., 2012, Principles of sediment transport applicable in tidal environments, *in* Davis, R.A., Jr., and Dalrymple, R.W., editors, Principles of tidal sedimentology: Dordrecht, Netherlands, Springer Science and Business Media, p. 19–34.

Westoby, M.J., Brasington, J., Glasser, N.F., Hambrey, M.J., and Reynolds, J.M., 2012, 'Structure-from-Motion' photogrammetry—a low-cost, effective tool for geoscience applications: Geomorphology, v. 179, p. 300–314.

Wheatley, D.F., Chan, M.A., and Sprinkel, D.A., 2016, Clastic pipe characteristics and distributions throughout the Colorado Plateau—implications for paleoenvironments and paleoseismic controls: Sedimentary Geology, v. 344, p. 20–33.

Wilcox, W.T., and Currie, B., 2008, Sequence stratigraphy of the Jurassic Curtis, Summerville, and Stump Formations, eastern Utah and northwest Colorado, *in* Longman, M.W., and Morgan, C.D., editors, Hydrocarbon systems and production in the Uinta Basin, Utah: Rocky Mountain Association of Geologists and Utah Geological Association Publication 37, p. 9–41.

Witkind, I.J., 1988, Geologic map of the Huntington 30' x 60' quadrangle, Carbon, Emery, Grand, and Uintah Counties, Utah: U.S. Geological Survey, Miscellaneous Investigations Series Map I-1764, 1 plate, scale 1:100,000.

Wright, J.C., Shawe, D.R., and Lohman, S.W., 1962, Definition of members of Jurassic Entrada Sandstone in east-central Utah and west-central Colorado: American Association of Petroleum Geologists Bulletin, v. 46, no. 11, p. 2057–2070.

Yonkee, W.A., and Weil, A.B., 2015, Tectonic evolution of the Sevier and Laramide belts within the North American Cordillera orogenic system: Earth-Science Reviews, v. 150, p. 531–593.